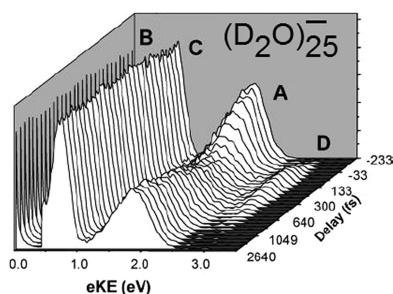


## Dynamics of Solvated Electrons in Clusters

Ryan M. Young<sup>†,§</sup> and Daniel M. Neumark<sup>\*,†,‡</sup><sup>†</sup>Department of Chemistry, University of California, Berkeley, California 94720, United States<sup>‡</sup>Chemical Sciences Division, Lawrence Berkeley National Laboratory, Berkeley, California 94720, United States

## CONTENTS

1. Introduction	5553
2. Methods for Investigating Solvent Cluster Anions	5554
2.1. Cluster Formation, Electron Attachment, and Mass Spectrometry	5554
2.2. Photoelectron Spectroscopy (PES) and Photoelectron Imaging (PEI)	5554
2.3. Infrared Spectroscopy	5556
2.4. Time-Resolved PES/PEI	5556
2.5. Theory of Electron Solvation in Clusters	5557
2.5.1. Dielectric Continuum models	5557
2.5.2. Quantum Chemistry, Pseudopotentials, and Molecular Dynamics	5557
3. Water	5557
3.1. Structural Studies of Water Cluster Anions	5558
3.2. Dynamics in Water-Based Cluster Anions	5561
3.3. Dynamics in Halide–Water Clusters	5563
4. Methanol	5564
5. Ammonia	5567
6. Acetonitrile and Primary Amides	5568
7. Benzene, Toluene, and Other Aromatic Solvents	5571
8. Tetrahydrofuran	5572
9. Summary and Outlook	5572
Author Information	5573
Corresponding Author	5573
Present Address	5573
Notes	5573
Biographies	5573
Acknowledgments	5573
References	5573

## 1. INTRODUCTION

Solvated electrons are a fundamental species to many areas of physical science. In addition to playing a key role in aqueous phase chemistry,<sup>1</sup> they have been implicated in a wide variety of phenomena including aerosol nucleation in the upper atmosphere,<sup>2</sup> the Birch reduction reaction in organic chemistry,<sup>3</sup> and a secondary role in the low-energy radiation damage to DNA.<sup>4</sup> They are important benchmark systems in

understanding the quantum mechanics of solvation as the simplest possible quantum solute. Starting from the first observations of the solvated electron in ammonia by Davy<sup>5</sup> in 1808 and Weyl<sup>6</sup> in 1864, the solvated electron, and more specifically, the hydrated electron,<sup>7,8</sup> have generated much curiosity and interest in the science community. Despite the vast body of work on the subject, several properties of the solvated electron are still not fully understood and many important questions remain. For example, the precise nature of the local solvation environment<sup>9–16</sup> and the variation of this environment with solvent are of considerable interest.<sup>17–19</sup>

Moreover, while the relaxation dynamics of the excess electron in water are well-studied,<sup>20–28</sup> often the experimental results can be difficult to interpret because of overlapping and convoluted processes.

These questions can be addressed in studies of excess electrons in clusters. Cluster science aims to track the properties of matter from the molecular to the macroscopic regimes.<sup>29,30</sup> This evolution is particularly amenable to study in charged clusters, where size-selection is straightforward.<sup>31</sup> Electrons in clusters can be investigated via solvent cluster anions of the type  $S_n^-$ , where  $S$  is the solvating species; clusters of this type are the most intuitive analog for a bulk solvated electron.<sup>32</sup> Clusters comprising a solvated halide anion or alkali atom provide an additional platform for studying electron solvation; one can, for example, photoionize or photodetach the dopant atom and inject the electron into the solvent network of the cluster.<sup>33</sup>

Many different types of experiments can be performed on these classes of clusters. Mass spectrometry can determine relative stabilities of various cluster sizes as well as separate charged clusters for spectroscopic interrogation. Infrared spectroscopy can be applied to determine the vibrational and electronic structure of the clusters, while photoelectron spectroscopy can access the relative energies of the cluster states and their ionized or detached products to understand the size-dependent energetics of electron solvation. Time-resolved photoelectron studies can also be applied to directly monitor both the populations and the energies of the states involved in a dynamical process, providing complementary information to transient absorption experiments in bulk liquids.<sup>32,33</sup> These species can also be studied in-depth by state-of-the-art theoretical methods, the results of which can be compared to experiment to extract information about cluster structures, energetics, and dynamics.

**Special Issue:** 2012 The Solvated Electron

**Received:** January 31, 2012

**Published:** June 28, 2012

With all the insight brought from the cluster studies, these methods are not without their shortcomings. With the exception of the alkali-doped clusters mentioned above, experiments typically involve anionic molecular beams which have very low particle densities, typically  $<10^6 \text{ cm}^{-3}$ , and often much lower when dealing with large clusters ( $n > 100$ ). These low target densities render the most common experimental tools for investigating solvated electrons in liquids such as transient absorption spectroscopy unusable, as they require measuring the (small) depletion of a parent signal. Instead, action spectroscopies, such as predissociation and photoelectron spectroscopy must be employed.

A more fundamental question in cluster studies of electron solvation is exactly how to extrapolate cluster measurements into meaningful comparisons to measured or calculated values in bulk matter. Classical electrostatic models of continuous dielectric media offer a guide to understanding the material- and size-specific properties of solvent clusters but are often not effective a priori. Nonetheless, qualitative predictions from these models have been used to explain electron binding energies<sup>34</sup> and internal conversion lifetimes<sup>35</sup> in various solvent clusters with reasonable success.

One concern in comparing cluster and bulk experiments is the ill-defined nature of the cluster temperature. In the majority of anion cluster experiments to date, the clusters are formed in a continuous or pulsed free jet expansion. The resulting temperature of the clusters is often approximated using the “evaporative ensemble” of Klots,<sup>36,37</sup> wherein a cluster temperature can be estimated based on its experimental lifetime and cohesion energy (the decrease in energy obtained after increasing size by one cluster unit). For the cluster to be seen in an experiment, it cannot have more internal energy than would be required for that unit to break apart (evaporate) before the observation time, thus allowing for an upper bound on the temperature. Anion beam temperatures can vary significantly based on the source conditions, but are typically around 100–200 K. The issue of cluster temperature has recently begun to be addressed<sup>38–40</sup> by the cluster community with the addition of radio frequency electrostatic traps and ion guides which allow for the anions to be collisionally equilibrated with a low-pressure buffer gas to attain a well-defined temperature prior to interrogation.

Another cautionary issue in extrapolating cluster studies to the bulk is that one is often comparing results from rather different experimental techniques. This gap has narrowed considerably in recent years with the development of photoelectron spectroscopy of liquid microjets.<sup>41,42</sup> It is now possible, for example, to measure the binding energy of solvated electrons in microjets and compare these results to electron binding energies in solvent cluster anions. This point is considered in more detail below and elsewhere in this volume.

There are still many open questions about the solvated electron in clusters. Possibly the most controversial in recent years is that of the location of the excess electron: does the electron localize on the surface or does it bind internally, perhaps in a cavity? This issue has been addressed in many recent experimental and theoretical studies, and is considered in detail throughout this article.

## 2. METHODS FOR INVESTIGATING SOLVENT CLUSTER ANIONS

Since solvated electron clusters  $S_n^-$  are the subject of much of this review, this section focuses on experimental and computa-

tional methodologies for probing the structure, energetics and dynamics of this class of clusters and how these properties change with size. Advancements in gas-phase experimental techniques have been crucial to the development of our understanding of electron solvation in mesoscopic systems and are at the forefront of modern research in this area. In a complementary fashion, computational chemistry has also provided molecular-level insight into the nature of these clusters. As always, the combination of theory and experiment gives the richest description of electron solvation in finite systems.

### 2.1. Cluster Formation, Electron Attachment, and Mass Spectrometry

The generation of solvated electron clusters typically begins in a supersonic molecular beam, in which a mixture of solvent species with rare gas atoms is expanded into vacuum. In a free jet, cluster formation is induced by cooling in the expansion. For anionic cluster beams, electrons must be introduced into the free jet expansion. This can be done using a hot filament coupled to an ionizer<sup>43</sup> or electron gun,<sup>44–46</sup> an electric discharge,<sup>47</sup> laser ablation of a solid target,<sup>48</sup> or by utilizing collisions between rare gas atoms in high Rydberg states and solvent clusters to drive electron attachment.<sup>49,50</sup> The mechanism of cluster formation depends on the details of the ion source. For example, in anion sources based on an electron gun, fairly high energy (200 eV to 1 keV) electrons are injected into the free jet, which can subsequently ionize the carrier gas, producing slow secondary electrons. These electrons can then produce negative ions by dissociative attachment of small molecules or by attachment to neutral clusters, which then cool by evaporation.

Early experiments<sup>51</sup> on solvated electron clusters were done using continuous ion beams, but in recent years, pulsed sources have gained popularity.<sup>52</sup> High-pressure and high-repetition rate pulsed valves, such as pulsed piezoelectric<sup>53</sup> or solenoid<sup>54</sup> valves are desirable for the formation of cold clusters and for ultrafast spectroscopy experiments, which utilize laser pulse trains from 0.5 to 10 kHz. Other approaches used to generate solvated electron clusters include gas aggregation sources<sup>40</sup> and the ionization/evaporation of solvent molecules from liquid jets in vacuum.<sup>55</sup>

Mass spectrometry plays a key role in anion cluster experiments, as it is used to characterize the distribution of clusters produced by the ion source and to select the ion of interest by mass. Continuous mass selectors such as quadrupole mass spectrometers or Wien filters can be used in conjunction with both continuous and pulsed ion sources and are the favored method in spectroscopy experiments based on continuous wave (cw) lasers.<sup>56</sup> Time-of-flight (TOF) mass spectrometry, generally based on the Wiley–McLaren<sup>57</sup> design, is often better-suited to experiments based on pulsed ion sources and pulsed lasers owing to the longitudinal (temporal) focusing properties of the spectrometer. Time-of-flight mass spectrometers often include an additional reflectron mass analyzer<sup>58,59</sup> to achieve higher mass resolution or to perform mass analysis on ion fragments produced in photodissociation experiments.<sup>44</sup>

### 2.2. Photoelectron Spectroscopy (PES) and Photoelectron Imaging (PEI)

Extensive experimental work on solvated electron clusters has been done using variants of anion photoelectron spectroscopy (PES),<sup>60</sup> the principles of which are illustrated in Figure 1.

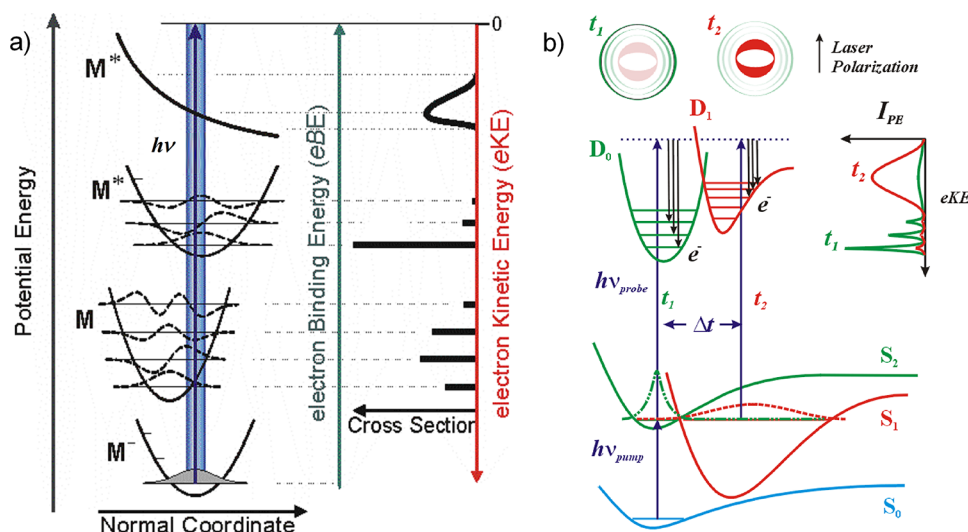


**Figure 1.** Schematics for one-photon anion photoelectron spectroscopy (a) and time-resolved photoelectron spectroscopy and imaging (b).

Mass-selected anions are photodetached by absorption of one or more photons to a neutral manifold of final states. The resulting electron kinetic energy (eKE) distribution is measured. For direct detachment with photon energy  $h\nu$ , the corresponding electron binding energy (eBE) is given by

$$eBE = h\nu - eKE \quad (1)$$

In PES, transitions to all neutral states energetically accessible via detachment of a single electron (one-electron transitions) are allowed. Within an electronic band, the distribution of vibrational levels produced by photodetachment is generally (but not always<sup>61,62</sup>) governed by the Franck–Condon overlap of the initial vibrational state of the anion ( $|v_i\rangle$ ) and final vibrational state of the neutral ( $|v_f\rangle$ ),

$$I \propto |\langle v_f | v_i \rangle|^2 \quad (2)$$

The photoelectron spectrum directly yields the electron affinity of the neutral when the transition between the vibrational ground states of the anion and neutral is resolved; this is equivalent to the adiabatic detachment energy (ADE) of the anion. When vibrational structure is not resolved, the ADE can be estimated from the onset of the photoelectron spectrum. Another very useful quantity is the vertical detachment energy (VDE), which corresponds to the eBE at the maximum of a photoelectron band. This quantity corresponds to the energy required to detach the electron with no nuclear rearrangement. The VDE is readily obtained even if no vibrational structure is resolved as is often the case in the photoelectron spectra of solvent cluster anions.

The photoelectron angular distribution (PAD) is also of interest. Assuming a randomly oriented cluster distribution, the PAD at a given eKE is given by<sup>63,64</sup>

$$\frac{d\sigma(eKE, \theta)}{d\Omega} = \frac{\sigma_{\text{total}}(eKE)}{4\pi} \sum_{i=1}^m \beta_{2i}(eKE) P_{2i}(\cos \theta) \quad (3)$$

where  $\theta$  is the angle between the emitted electron and the laser polarization,  $m$  is the number of photons absorbed in the process,  $\sigma_{\text{total}}$  is the total photodetachment cross section,  $\beta_{2i}$  are the anisotropy parameters containing the angular momentum information, and  $P_{2i}$  are the even Legendre polynomials. For a single-photon process,  $\beta_2$  ranges continuously between +2 and -1, representing an outgoing  $p$ -wave and an  $s+d$  wave,

respectively. Isotropic emission results in  $\beta_2 = 0$ . Higher photon-order photodetachment results in the transfer of additional angular momentum which allows the  $\beta$  parameters to take on other values beyond this range.

The first anion photoelectron spectroscopy experiments used cw intracavity radiation to photodetach negative ions and a hemispherical analyzer to measure the electron kinetic energy distribution.<sup>65</sup> The high circulating power of the intracavity laser (>100 W) is needed to compensate for the low ion density in these experiments and the restricted angular acceptance of the hemispherical analyzer. Originally, detection was not multiplexed; only one kinetic energy was collected at a time, but the later incorporation of position-sensing microchannel plate (MCP) detectors enabled photoelectron collection over a wider range of eKE.<sup>66</sup> An eKE resolution of 5 meV is achievable with this arrangement.<sup>67</sup> A photoelectron spectrometer of this general design was used by Bowen<sup>46,51</sup> to obtain the first photoelectron spectra of  $(\text{H}_2\text{O})_n^-$  and  $(\text{NH}_3)_n^-$  clusters.

Many anion photoelectron spectrometers built since the 1980s use pulsed lasers for photodetachment, in part because these lasers can more easily produce higher photon energies than intracavity cw lasers. These spectrometers generally use time-of-flight methods for electron energy analysis. In the simplest implementation of photoelectron TOF, the photoelectrons travel through a field-free flight region, typically a shielded  $\mu$ -metal tube, 50–100 cm long, where they spread in space according to their kinetic energies imparted upon detachment, and the differences in their arrival times at a microchannel plate detector are converted into measured kinetic or binding energy spectra.<sup>68,69</sup> TOF photoelectron analysis is multiplexed, in that signal is measured over the entire eKE range for each laser shot. The energy resolution can be as high as 8–10 meV. The collection efficiency is determined by the solid angle subtended by the MCP detector at a fixed distance from the laser interaction region. For 70 mm diameter MCPs and a flight length of 100 cm, the collection efficiency is  $10^{-3}$ . The PAD can be extracted by measuring TOF spectra with the laser polarization parallel and perpendicular to the axis of the flight tube.<sup>70</sup> Field-free TOF was used by Johnson and co-workers<sup>71</sup> to measure PE spectra of  $(\text{H}_2\text{O})_n^-$  clusters.

The collection efficiency of a TOF spectrometer can be dramatically increased using a “magnetic bottle” analyzer, comprising an inhomogeneous, axially symmetric magnetic field from a permanent magnet and a long solenoid flight tube.<sup>72–74</sup>

The magnetic field makes the electrons traveling toward the detector parallel by coupling to their axial velocity components via the Lorentz force. This translates photoelectron speed to a TOF but with a much higher collection efficiency, around ~50% owing to the enhanced acceptance angle ( $2\pi$  steradians). One generally cannot obtain PADs using a magnetic bottle TOF spectrometers. Moreover, while the intrinsic energy resolution of a magnetic bottle analyzer is comparable to field-free TOF, the energy resolution in an anion beam experiment using beam energies of 1–2 keV is much worse owing to Doppler effects<sup>75</sup> unless the anions are decelerated significantly prior to photodetachment. Spectrometers with magnetic bottle analyzers have been used by Kaya and co-workers<sup>48,76</sup> to measure PE spectra of (benzene)<sub>n</sub><sup>−</sup>, (toluene)<sub>n</sub><sup>−</sup>, and (CH<sub>3</sub>CN)<sub>n</sub><sup>−</sup> clusters, and by Maeyama et al.<sup>77,78</sup> to study electron solvation in clusters of primary amides.

Another more recent approach to anion photoelectron spectroscopy, photoelectron imaging (PEI), was pioneered by Bordas,<sup>79,80</sup> Sanov,<sup>81,82</sup> and their co-workers. These experiments build upon the photofragment and photoelectron imaging studies first carried out by Chandler<sup>83,84</sup> and Helm,<sup>85</sup> respectively, and the discovery of velocity-map imaging (VMI) by Parker and co-workers,<sup>86</sup> which greatly improved the energy resolution of both photoion and photoelectron imaging.

In anion PEI, mass-selected ions are photodetached in a DC field of several hundred V/cm and the electrons are accelerated toward an MCP detector coupled to a phosphor screen. The resulting image of the photoelectrons is recorded by a CCD camera. The image is the projection of the three-dimensional photoelectron velocity distribution onto a two-dimensional plane; the original 3-D distribution can be recovered using well-established methods,<sup>87,88</sup> yielding the photoelectron kinetic energy and angular distributions. Photoelectron imaging offers high collection efficiency with a typical energy resolution of 2–5%. The Neumark group has used PEI to obtain photoelectron kinetic energy spectra and angular distributions of (H<sub>2</sub>O)<sub>n</sub><sup>−</sup>, (CH<sub>3</sub>OH)<sub>n</sub><sup>−</sup>, (CH<sub>3</sub>CN)<sub>n</sub><sup>−</sup>, and (THF)<sub>n</sub><sup>−</sup> clusters.<sup>89–92</sup>

### 2.3. Infrared Spectroscopy

Anion photoelectron spectroscopy yields electron binding energies and, in many cases, resolved vibrational progressions for polyatomic molecules and some clusters. However, for complex cluster anions such as S<sub>n</sub><sup>−</sup> clusters, PES typically does not yield vibrational structure, primarily because the anion and neutral equilibrium geometries are very different, resulting in long progressions in low frequency modes that are not resolved in the PE spectrum. Infrared (IR) action spectroscopy, on the other hand, has been quite successful in generating vibrationally resolved spectra in clusters as large as (H<sub>2</sub>O)<sub>50</sub><sup>−</sup> (ref 93.) and therefore serves as an excellent structural probe of S<sub>n</sub><sup>−</sup> clusters and related species.

The most general variant of IR action spectroscopy for studying anionic clusters is IR predissociation spectroscopy.<sup>94,95</sup> Here, absorption of one or more infrared photons is detected through dissociation of either a pure solvent cluster anion or a cluster complexed to one or more Ar atoms or another weakly bound species



These experiments are typically carried out in a tandem mass spectrometer, in which parent ions are mass-selected prior to interacting with the IR source, and either depletion of parent ions or production of daughter ions is monitored with a second mass analyzer.

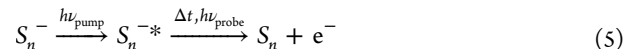
The binding energy of an Ar atom to a cluster anion is much smaller than the binding energy for a solvent molecule S, so absorption of a single IR photon is sufficient to induce Ar evaporation. As a result, experiments with Ar-tagged clusters can be readily performed using table-top IR lasers, which can now extend down to IR frequencies as low as 600 cm<sup>−1</sup>.<sup>96</sup> In a recent advance by the Johnson group,<sup>97</sup> double resonance spectroscopy using two infrared pulses has been used to unravel the contributions of multiple isomers of small water cluster anions to the infrared spectrum.

For cold, bare cluster anions, multiple IR photon absorption is often needed to evaporate a solvent molecule. Experiments on these species have been performed with considerable success using tunable infrared free electron lasers, for which the peak power is substantially higher than for table-top systems.<sup>98</sup> An alternative approach developed by the Williams group<sup>99,100</sup> measures infrared spectra of bare ions in a Fourier-transform ion cyclotron resonance spectrometer, where ions excited by a single tunable infrared photon dissociate owing to additional internal energy from blackbody radiation.<sup>101</sup>

### 2.4. Time-Resolved PES/PEI

The experimental methods described above probe the energetics and structure of solvent cluster anions and related species. Time-resolved dynamics in these clusters are also of considerable interest, particularly as a point of comparison with ultrafast experiments on bulk solvated electrons. Time-resolved photoelectron spectroscopy (or imaging), TRPES (or TRPEI), is a powerful method for probing femtosecond dynamics in clusters. Several reviews<sup>102–104</sup> have been written on this subject. TRPES is well-suited to the study of anions because the binding energy of the excess electron is generally below typical photon energies produced by table-top femtosecond laser systems.

A typical time-resolved photoelectron experiment on mass selected anions is



with more information provided in Figure 1. The anion is electronically excited with a femtosecond laser pulse (called the “pump” pulse). The nascent nonstationary state then evolves on the excited state potential energy surface until a second femtosecond laser pulse (the “probe” pulse) detaches the electron into the continuum, and the resulting photoelectron spectrum is collected. The time delay  $\Delta t$  between the pump and probe pulses can be precisely controlled, allowing the dynamics to be monitored in real-time. The time-evolving photoelectron spectrum can probe dissociation on the excited state, vibrational wave packet motion on the excited or ground electronic states, and radiationless transitions between the initially excited state and lower-lying electronic states; each of these processes has its own signature in TRPES.<sup>104</sup> The ability to follow radiationless transitions versus pump–probe delay provides an extremely useful and general probe of relaxation in

electronically excited solvated cluster anions, as described in more detail below.

Energy resolution must, invariably, be sacrificed for temporal resolution due to the energy spread of the femtosecond pulses, but solvated electron clusters generally exhibit very wide photoelectron spectra regardless of the laser bandwidth so the loss of information is minimized. A relative resolution of  $\Delta E/E \approx 5\%$  is easily achievable even with  $\sim 30$  fs laser pulses. Harmonic generation or optical parametric amplification is employed to provide the necessary photon energies with minimal pulse stretching. The dynamical process of interest dictates the temporal resolution; this can vary from sub-100-femtoseconds for internal conversion processes to several nanoseconds for electron solvation following charge injection from iodide. Modern tabletop femtosecond laser systems with pulse widths of 30 fs are perfectly suited to study these processes.

## 2.5. Theory of Electron Solvation in Clusters

Theoretical studies on solvated electron clusters have been invaluable to understanding their structures, energetic and dynamics. While infrared and photoelectron spectroscopies can offer a great deal of insight into the binding motifs of smaller solvated electron clusters, the information they offer becomes more convoluted and less-well resolved for larger cluster sizes. Thus being able to visualize their structure and quantify aspects of their bonding becomes necessary to understand the transition from the molecular to the bulk regimes.

**2.5.1. Dielectric Continuum models.** Ideally, a model for studying the binding and dynamics of an excess electron in a cluster would include both size and material effects. Dielectric continuum (DC) theories<sup>34,105,106</sup> offer a first approximation to many properties of solvated electron clusters based on their size and the properties of the bulk liquid. These models assume a spherical cluster of uniform density with the sphere's dielectric properties describable by a small number of parameters which can be measured or estimated independently. The obvious drawback is the neglect of molecularity, which for small clusters is clearly very important. However, good qualitative agreement has been found with a number of these models and, with the proper choice of parameters, some properties can be predicted quantitatively.<sup>46,48,76,107</sup> For example, by modeling the solvated electron cluster as an excess charge within a cavity inside a dielectric sphere of radius  $R$ , the VDEs of solvent cluster anions can be approximated in cgs units by<sup>34,108</sup>

$$\text{VDE}(n) = \frac{e^2}{2} \left( 1 + \frac{1}{\epsilon_\infty} - \frac{2}{\epsilon_s} \right) \left( \frac{1}{a_0} - \frac{n^{-1/3}}{r_0} \right) \quad (6)$$

where  $a_0$  is the electron cavity size,  $r_0$  is the average molecular radius,  $\epsilon_\infty$  and  $\epsilon_s$  are the optical and static dielectric constants, respectively, and  $n$  is the cluster size ( $R^3 = r_0^3 n$ ). The intercept of this equation is a prediction of the bulk electron binding energy. Anionic solvent cluster VDEs fit well to lines when plotted versus  $n^{-1/3}$ , so the DC theories offer a good conceptual framework, if often a poor predictive model. It should be noted that the supposition of the charge localized within a dielectric sphere implicitly assumes the validity of the cavity model for the solvated electron, an assumption that is generally accepted, but has been called into question.<sup>11–16</sup> The reader is referred to other works in this volume on the cavity nature of the solvated electron.

**2.5.2. Quantum Chemistry, Pseudopotentials, and Molecular Dynamics.** Solvent cluster anions present many

interesting computational challenges from the perspective of quantum chemistry, as detailed in several review articles.<sup>109–111</sup>

Most theoretical work to date has focused on water cluster anions, although methanol and other solvent cluster anions have recently been treated as well. Pure quantum chemistry approaches based on ab initio electronic structure calculations are challenging because the wave function for the excess electron in these clusters tends to be quite diffuse, thus requiring a large basis set to describe the electron and its interactions with solvent species in the cluster.<sup>112,113</sup> This situation is complicated by the presence of multiple low-lying isomers with similar energies, particularly in the case of water cluster anions.<sup>114,115</sup> Hence, when a minimum energy structure is located, it is often an open question as to whether this structure corresponds to a local or global minimum. As a result, most fully quantum electronic structure calculations have been carried out on small clusters with ten or fewer solvent molecules, although calculations on considerably larger cluster anions are becoming more frequent.<sup>78,116–118</sup>

An alternative theoretical approach to solvent cluster anions is based on one-electron models.<sup>109</sup> These calculations generally make use of pseudopotentials that represent the interaction of an electron with a single solvent molecule, with empirical corrections added in to confine the electron, account for long-range electron–solvent interactions, etc.<sup>13,106,119–121</sup>

The electron–solvent interaction, governed by the pseudopotential, is treated quantum mechanically, while the remaining interactions are treated either classically or with a mixture of quantum and classical mechanics. The construction of suitable pseudopotential functions is nontrivial, as it involves designing an analytical expression that is designed to fit calculated energies for the electron–solvent interaction. Several of these one-electron models allow for polarization of the solvent by the excess electron.<sup>109</sup> The Drude model goes one step further and accounts for dispersion interactions between the electron and solvent molecules.<sup>122</sup> However, once a suitable one-electron model is developed, it can be applied to large cluster anions comprising hundreds of solvent molecules<sup>123,124</sup> as well as to the spectroscopy and dynamics of electrons in bulk solvents.<sup>25,125–127</sup> Calculations of this type, for example, were used in the pioneering work of Landman, Jortner, and co-workers in which the existence of internal and surface-bound electrons in water cluster anions was predicted,<sup>108</sup> and in similar work on ammonia cluster anions by Klein and co-workers.<sup>128</sup>

Several recent theoretical treatments have explored dynamics in solvent cluster anions, with particular focus on how electrons attach to neutral clusters and whether an excess electron initially inside a cluster remains inside or moves toward the surface. Fully quantum mechanical ab initio molecular dynamics have been performed on clusters as large as  $(\text{H}_2\text{O})_{35}^-$ ,<sup>129</sup> while calculations based on one-electron models have explored dynamics in considerably larger clusters.<sup>130–132</sup> As discussed in specific examples below, these calculations have highlighted the role of cluster temperature on the binding motif and energetics of the excess electron.

## 3. WATER

The body of work on the hydrated electron in the bulk,  $e_{\text{aq}}^-$ , is beyond the scope of this article, but is covered elsewhere within this volume. The generally accepted picture has  $e_{\text{aq}}^-$  occupying a quasi-spherical cavity formed by the water network with a radius of about 2.4 Å.<sup>9,125,133</sup> The cavity formed by the solvent

acts as a potential trap for the electron, deep enough to bind the electron significantly and to support several bound, quasi-degenerate excited electronic states.<sup>126</sup> The electron is stabilized predominantly by  $e^- \cdots \text{HO}$  interactions with the  $\sim 4\text{--}6$  water molecules<sup>10,121,134</sup> that form the cavity,<sup>135</sup> but also electrostatically by the outer solvation layers.

The electronic absorption spectrum of  $e_{\text{aq}}^-$  is broad and featureless, peaking around 720 nm (1.7 eV).<sup>136</sup> This band is primarily attributed to a promotion from an  $s$ -like ground state within the cavity to a manifold of  $p$ -like states whose degeneracy is split by the fluctuations of the solvent cavity.<sup>125,157</sup> The relaxation mechanism for the excited state has been extensively studied.<sup>22</sup> After excitation, the  $p$ -like state can be stabilized prior to internal conversion (IC) and subsequent ground state relaxation.<sup>32,33</sup>



This mechanism is shown schematically in Figure 2. The time scales of each of these processes are a matter of debate.

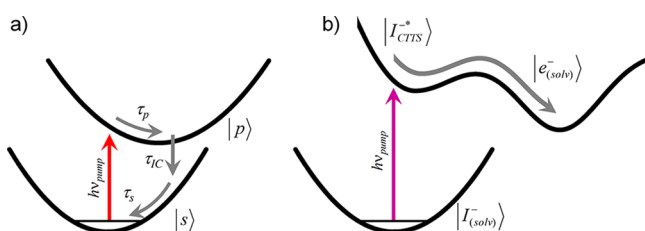


**Figure 2.** Energy level diagrams for the relaxation dynamics of bulk solvated electrons (a) and charge-transfer-to-solvent dynamics in liquids (b).

Transient absorption experiments<sup>21,28,113,138–141</sup> show that the excited state of  $e_{\text{aq}}^-$  decays rapidly with three distinct time constants which are compatible with two competing schemes. The “adiabatic” model<sup>25,28,141–143</sup> proposes that the most rapid time scale ( $\sim 50$  fs) corresponds to relaxation along the excited  $p$ -state surface ( $\tau_p$ ), while internal conversion ( $\tau_{\text{IC}}$ ) takes several hundred femtoseconds, and the relaxation along the unequilibrated  $s$ -state is the slowest step ( $\sim 1$  ps). Alternatively, the “nonadiabatic” model<sup>21,24,140</sup> suggests that the fastest observable time scale of  $\sim 50$  fs is the internal conversion step, and that the slower steps belong to relaxation on the ground state.

Another series of experiments focuses on the hydration dynamics of electrons formed in solution by multiphoton ionization of water or charge-transfer from a solvated anion;<sup>122,144–146</sup> the latter process involves ultraviolet excitation of the well-known charge-transfer-to-solvent (CTTS) bands for aqueous anions.<sup>147</sup> The electron generated by either mechanism can recombine with its parent or it can diffuse away to become a true solvated electron, requiring the solvent network to relax around it. These dynamics are notably slower than excited state relaxation, typically lasting several picoseconds. Sections 3.1 and 3.2 present the cluster analogs of both types of dynamics experiments.

### 3.1. Structural Studies of Water Cluster Anions

Water cluster anions,  $(\text{H}_2\text{O})_n^-$ , were first observed by Haberland in 1984,<sup>148</sup> more than 20 years after the discovery of the bulk hydrated electron.<sup>102</sup> While a single water molecule cannot bind an excess electron on its own, the water dimer anion was observed to be stable, in that it remains detectable long enough to be measured ( $>100 \mu\text{s}$ ), indicating a positive

electron affinity.<sup>51,71,148</sup> Subsequent experiments have shown a relative enhancement of the  $n = 2, 6, 7,$  and  $11$  peaks in the mass spectra which suggests that these sizes are more stable relative to others.<sup>71,149–151</sup> Interestingly, these “magic numbers” were not seen in a more recent experiment by Scheier,<sup>152</sup> in which water cluster anions were formed by attachment to water-doped He droplets.

The first spectroscopic characterization of water cluster anions came from the photoelectron spectra measured by Bowen<sup>51</sup> for  $(\text{H}_2\text{O})_n^-$  up to  $n = 69$ ; subsequent work by Johnson<sup>71</sup> focused on smaller clusters. The PE spectra of smaller water cluster anions, up to  $n = 10$ , exhibit sharp peaks at low binding energies. Beginning at  $n = 11$ , the peaks broaden and shift to higher binding energies continuously, up to 1.96 eV for  $n = 69$ . The photoelectron spectra of larger  $(\text{H}_2\text{O})_n^-$  clusters are characterized by their broad, asymmetric line shape. The VDEs increase gradually with cluster size, scaling linearly with the inverse cluster radius, or as  $n^{-1/3}$ , as would be expected for an internally bound electron. Extrapolating to infinite cluster size along this coordinate yields an estimate for the bulk electron binding energy of  $\sim 3.25$  eV.

Neumark and co-workers<sup>153,154</sup> measured photoelectron spectra of  $(\text{H}_2\text{O})_n^-$  clusters generated in a pulsed molecular beam and found that a second binding motif or “isomer” with substantially lower VDE was formed at higher stagnation pressures (colder expansion conditions) of the argon carrier gas. Both the original feature observed by Bowen<sup>51</sup> and the new feature were shown to coexist, with the new isomer dominating as the stagnation pressure of the Ar carrier gas was raised from 30 psig to 70 psig. Representative photoelectron spectra are shown in Figure 3 for  $(\text{D}_2\text{O})_{50}^-$ . The new feature has a

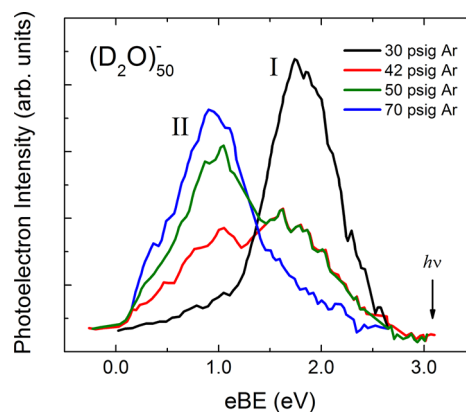


**Figure 3.** Photoelectron spectra for  $(\text{D}_2\text{O})_{50}^-$  taken with 3.10 eV and at different stagnation pressures of argon, adapted from Verlet et al.<sup>89</sup>

significantly lower binding energy, ranging from 0.51 eV at  $n = 11$  to 1.26 eV at  $n = 200$ . The distinct nature of this species motivated recasting the original feature seen by Bowen as “isomer I” and calling the new feature “isomer II”. Photoelectron spectra for both isomers were seen for clusters as large as  $n = 200$ . A third even more weakly bound feature termed “isomer III” was also observed for  $(\text{D}_2\text{O})_n^-$  clusters,  $n = 11\text{--}50$ , at the highest stagnation pressures with a nearly constant binding energy of  $\sim 0.2$  eV. Additional evidence for multiple isomers was seen in more recent PE spectra reported by Bowen.<sup>155</sup>

Figure 4 summarizes the size-dependent VDEs reported for  $(\text{H}_2\text{O})_n^-$  clusters from the Neumark group and for other

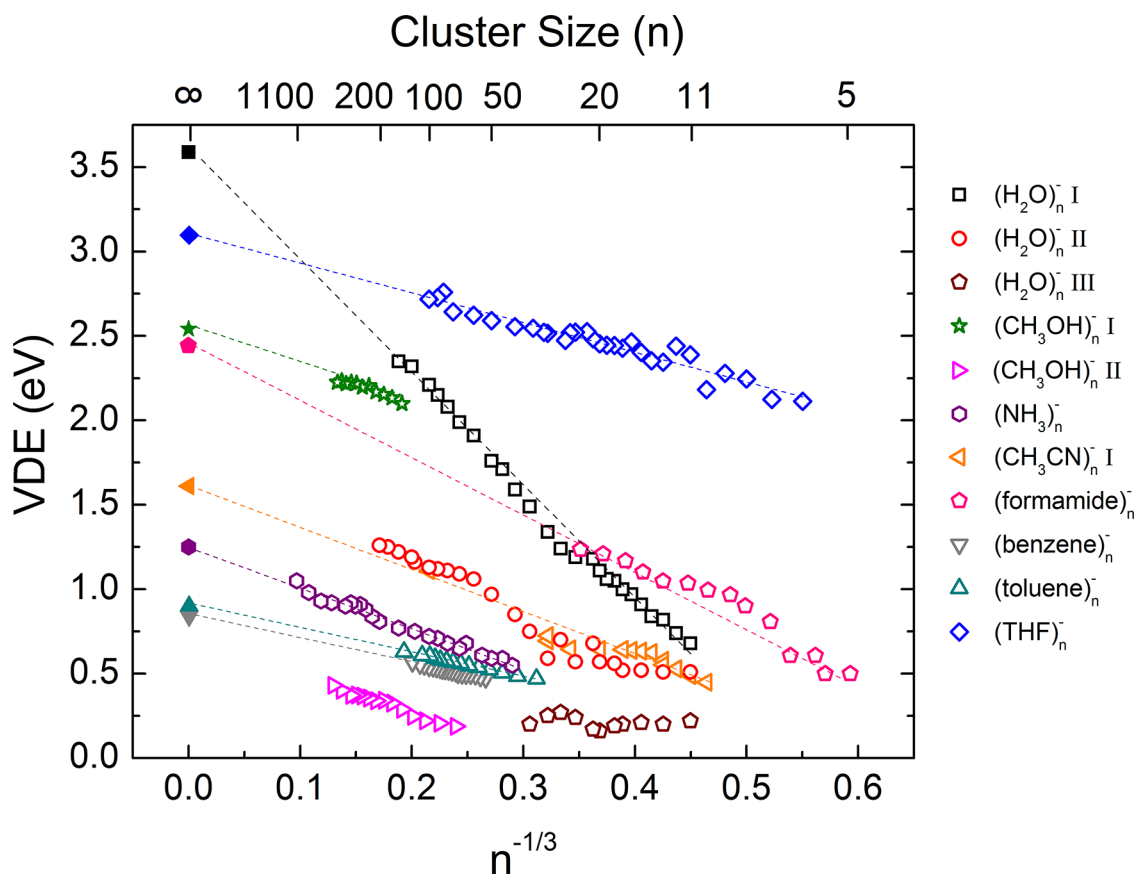


**Figure 4.** Vertical detachment energies versus  $n^{-1/3}$  for the various solvents considered here:  $(\text{H}_2\text{O})_n^-$  isomer I (black squares), isomer II (red circles), isomer III (maroon pentagons), adapted from Verlet et al.,<sup>89</sup>  $(\text{CH}_3\text{OH})_n^-$  isomer I (green stars), isomer II (pink right-facing triangles) adapted from Kamrath et al.,<sup>221</sup>  $(\text{NH}_3)_n^-$  (purple hexagons) adapted from Sarkas et al.<sup>46</sup> and Lee et al.,<sup>242</sup>  $(\text{CH}_3\text{CN})_n^-$  isomer I (orange left-facing triangles),  $(\text{benzene})_n^-$  (gray downward triangles),  $(\text{toluene})_n^-$  (teal upward triangles) adapted from Mitsui et al.,<sup>48,76</sup>  $(\text{formamide})_n^-$  (pink pentagons) adapted from Maeyama, et al.,<sup>77</sup> and  $(\text{THF})_n^-$  (blue diamonds) adapted from Young et al.<sup>92</sup> Solid markers indicate the extrapolated bulk limits.

solvated electron clusters described later in this paper. The VDEs are plotted versus  $n^{-1/3}$ , which should be roughly proportional to the inverse of the cluster radius. The VDEs for isomer I largely agree with those of Bowen's group,<sup>155</sup> although they appear to increase faster with cluster size. Indeed, a change in slope is observed around  $n = 25$ – $35$ ; extrapolating from this size onward yields a higher estimate of the bulk vertical binding energy of about  $\sim 3.6$  eV.

The water cluster anions reported in Bowen's original work were attributed to clusters with internally solvated electrons, an assignment supported by their VDE extrapolation to 3.25 eV, as this value was considered a reasonable value for the bulk hydrated electron.<sup>51,156</sup> The observation by Neumark of two coexisting isomers over a wide size range provided further support for this assignment; based on the calculations by Barnett et al.<sup>108</sup> that found that surface-bound electrons should exhibit a lower binding energy than internal states, isomer II was assigned to a surface state of the water cluster, making isomer I a proper candidate for the internally solvated electron. However, while there is currently general agreement that isomer II is a surface state, the nature of isomer I has engendered more controversy,<sup>123</sup> some of which is touched on below.

Further insights into the nature of isomer I have come from controlling the ion temperatures using either a radio frequency trap or changing the carrier gas. By cooling  $(\text{H}_2\text{O})_n^-$  and

$(\text{D}_2\text{O})_n^-$  clusters to 10 K and fitting the photoelectron spectra to multiple Gaussian–Lorentzian profiles, von Issendorf and co-workers<sup>40</sup> found that what had previously been deemed “isomer I” actually comprises two different binding motifs at low temperatures. The more tightly bound feature is associated with the internally bound electron on the basis of magic numbers of the low-temperature mass spectrum. This species extrapolates to a bulk VDE of  $\sim 4$  eV, higher than previous estimates. Recently, the Neumark group<sup>157</sup> produced water cluster anions in adiabatic expansions with neon carrier gas, which is known to be less efficient than argon at deactivating vibrational excitation in large molecules.<sup>158,159</sup> The resulting photoelectron spectra showed only isomer I clusters for all Ne stagnation pressures studied, up to 250 psig.

Related studies on alkali-doped water clusters by Fuke,<sup>160</sup> Hertel,<sup>161</sup> and others<sup>162,163</sup> also give estimates of the bulk binding energies. In these studies, the valence electron on the alkali dopant spontaneously dissociates from the atom by the solvent cluster,  $\text{M}(\text{H}_2\text{O})_n \rightarrow \text{M}^+(\text{H}_2\text{O})_n^-$  (where  $\text{M} = \text{Na}, \text{Cs}$ ), forming an analog of the hydrated electron cluster. Photoionization of these clusters shows that the ionization potentials (IPs) rapidly level off, becoming approximately constant for relatively small aggregates (e.g.,  $n = 6$ , for Na).<sup>164</sup> Extrapolating these IPs yields a bulk binding energy of  $\sim 3.2$  eV. Williams and co-workers<sup>165,166</sup> have investigated the inverse process, electron capture by clusters containing multiply charged metal cations,

in experiments that probe the energetics and solvation motif of the added electron.

The electron binding motif for small water cluster anions was addressed more directly by Johnson and co-workers in a series of infrared spectroscopy studies on these species. These experiments were carried out in the OH stretching region ( $3000\text{--}4000\text{ cm}^{-1}$ )<sup>115,167</sup> and water bend region ( $1500\text{--}1700\text{ cm}^{-1}$ )<sup>167–169</sup> using Ar-mediated infrared predissociation spectroscopy (eq 4). The most striking result from these studies is the observation of an unusual binding motif shown in Figure 5a

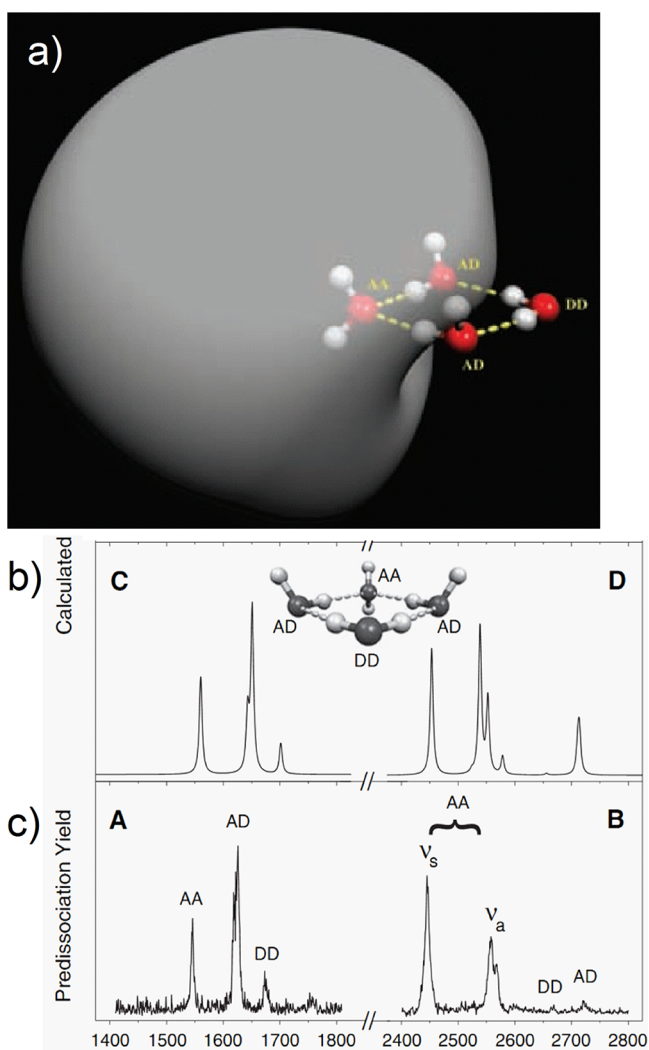


**Figure 5.** (a) SOMO of the cyclic water tetramer anion calculated with DFT using B3LYP/6-311++G\*\*(*sp*) showing the double acceptor motif. (b) Calculated vibrational spectrum for  $(\text{H}_2\text{O})_4^-$  (feature C) and for  $(\text{D}_2\text{O})_4^-$  (feature D) at the same level of theory. (c) Analogous experimental spectra for  $(\text{H}_2\text{O})_4^- \cdot \text{Ar}_5$  and  $(\text{D}_2\text{O})_4^- \cdot \text{Ar}_{10}$ , showing good agreement with theory. Adapted from ref 168. Reprinted with permission from AAAS.

for  $(\text{H}_2\text{O})_4^-$ . This structure is based on the experimental and calculated spectra in Figures 5b and c. Here, the excess electron resides in a diffuse orbital bound primarily to a single water molecule in a double-acceptor (AA) hydrogen-bonding configuration with both of its H-atoms pointing into the electron density. The bend vibration for this water molecule (AA in Figure 5c) at  $1550\text{ cm}^{-1}$  is significantly red-shifted from its neighbors. Evidence for the AA binding motif is seen for

clusters as large as  $n = 24$  in Ar-tagging experiments.<sup>170</sup> The diffuse orbital characteristic of AA binding is likely to lie outside the cluster, so the observation of the AA infrared signature suggests surface-binding of the excess electron up to this cluster size. Experiments using a tunable IR free electron laser to induce infrared multiple-photon dissociation of bare  $(\text{H}_2\text{O})_n^-$  anions showed that while the AA feature diminishes with increasing cluster size, it was visible up to  $n = 35$  and became much less distinct in the  $n = 35\text{--}50$  size range.<sup>93</sup> The transition around  $n = 25\text{--}35$  coincides with the change in the VDE versus  $n^{-1/3}$  slope, possibly indicating the onset of a fundamental change in electron binding around this size.

Johnson<sup>131,132</sup> has used action spectroscopy in a slightly higher energy regime to measure electronic absorption spectra of  $(\text{H}_2\text{O})_n^-$  clusters. These photodestruction experiments probed absorption from 0.5 to 2 eV for the cluster size range  $n = 15\text{--}40$ . The results, shown in Figure 6, show that the peak

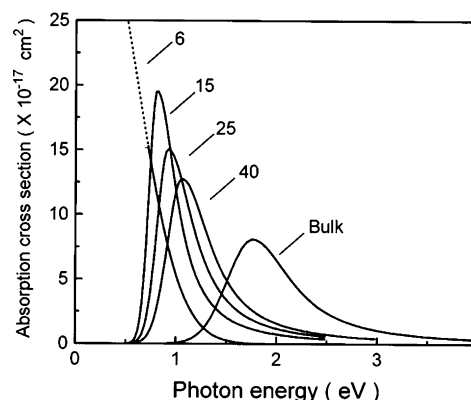


**Figure 6.** Electronic absorption spectra for  $(\text{H}_2\text{O})_n^-$  out to  $n = 40$ . Reprinted with permission from ref 171. Copyright 1997 American Institute of Physics.

maximum blue-shifts with increasing size over this range, from 0.8 to 1.1 eV, and appear to be converging to the spectrum of  $e_{\text{aq}}^-$ . The lineshapes of the absorption spectra agree very well with the measured bulk spectrum and are similar to those of the photoelectron spectra. Moment analysis<sup>133,171</sup> of these spectra suggest the electron is more diffuse than in the bulk, having a radius of gyration of  $\sim 3.4\text{--}3.0\text{ \AA}$  over the size range measured (compare to  $\sim 2.4\text{ \AA}$  in liquid water). The size-dependent evolution of the spectrum is the subject of a 2001 review by Coe.<sup>156</sup>

A large body of theoretical work has been carried out on water cluster anions, much of which is summarized elsewhere within this volume. The discussion here will be restricted to studies of larger clusters ( $>10$  water molecules) for which the primary goal is to understand localization of the excess electron and finding the signatures of surface vs internal solvation. This question was first addressed by Barnett et al.<sup>93,129,144</sup> using quantum path-integral Monte Carlo simulations.<sup>105,108,172</sup> This work found that surface binding was energetically lower in small clusters,  $8 \leq n < 32$ , while internal solvation was favored for larger clusters,  $n \geq 64$ . Calculated VDEs for internal states were roughly twice those of surface-bound electrons, suggesting that the binding energies would provide the experimental evidence for the expected internally solvated electrons.

Shortly after the experimental observation of isomer II, Rossky and co-workers<sup>123</sup> showed using mixed quantum-classical simulations that the trends in the photoelectron and

optical absorption spectra for water cluster anions could be explained by assignment of the high-binding energy states to surface-binding states, and that internalization does not occur until between  $n = 100$  and  $n = 200$ . However, isomer II was also not explicitly considered in this study, and the calculated VDEs lie in between the experimental values for each isomer.<sup>89</sup> Several other groups have reported electronic structure calculations in order to explore various electron binding motifs.<sup>117,173–176</sup>

The photoelectron angular distributions from isomer I and II clusters have also been explored.<sup>177</sup> The clearest observed trend is that for isomer I clusters in the size range  $n = 30–60$ , direct, one-photon detachment at 395 nm yields considerably more anisotropic distributions than resonant two-photon detachment at 790 nm, with average values for  $\beta_2$  of 0.75 and 0.12, respectively. The  $p$ -like distributions at 395 nm indicate detachment from an  $s$ -like orbital, whereas the nearly isotropic distributions from resonant two-photon detachment suggest an intermediate excited state with considerable  $p$ -character.<sup>63,178</sup> These observations are consistent with assigning the electronic absorption at 790 nm<sup>171</sup> to a  $p \leftarrow s$  transition of the excess electron. Interestingly, a similar trend was not seen for isomer II clusters, where direct detachment at 790 nm and resonant two-photon detachment at 1650 nm yield similarly anisotropic angular distributions ( $\beta_2 \approx 1.2$ ) over a wide size range,  $n = 50–130$ .

Recent theoretical work<sup>118,132</sup> has investigated the correlation between the radius of gyration of the excess electron, its VDE, and its position relative to the cluster surface. Jungwirth<sup>118</sup> and Herbert<sup>132</sup> have shown that the solvated electron VDE is strongly correlated with its radius of gyration, with more localized electrons being more strongly bound, as seen in Figure 7. It is worth noting that the same correlation between VDE and radius of gyration was observed in negatively charged methanol clusters.<sup>131</sup>

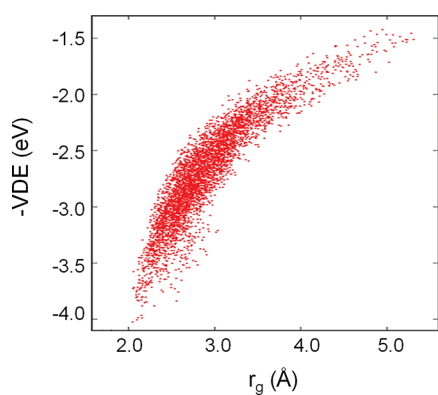


**Figure 7.** VDE vs electron radius of gyration in water cluster anions, showing an inverse relationship. Reprinted with permission from ref 110. Copyright 2010 American Chemical Society.

The influence of cluster temperature has been the subject of numerous theoretical studies by Jungwirth,<sup>110,118,129,179</sup> and Rossky.<sup>130</sup> Simulations show that electron attachment to cold water clusters (20–50 K) preferentially forms surface-bound isomers, as the solvent fluctuations do not have sufficient amplitude to allow the electron to sample the interior of the cluster. For example, for  $(\text{H}_2\text{O})_{32}^-$  with a bath temperature of 20 K, no internalization occurs and only surface-bound states are seen, but at 300 K, some internalization takes place within

$\sim 1.5$  ps.<sup>129</sup> Most recently, Herbert and co-workers<sup>132</sup> have proposed a new isomer as an intermediate between surface and truly internal states: a partially embedded electron where the electron density is significant within the solvent network. Representative structures for each of the isomers of  $(\text{H}_2\text{O})_{40}^-$  in this study are shown in Figure 8. Fully internally bound

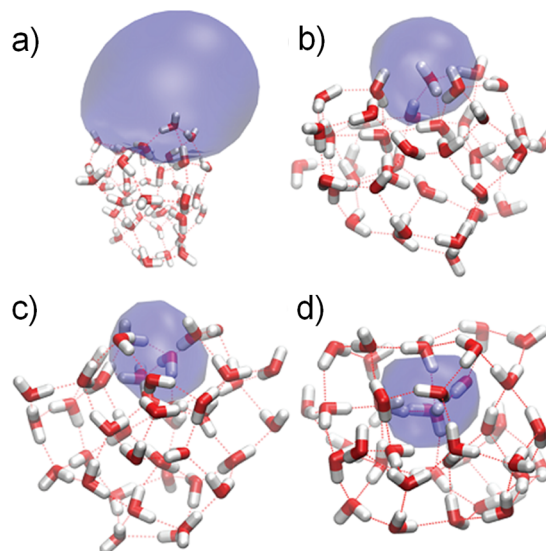


**Figure 8.** Representative structures from each of the four isomers in  $(\text{H}_2\text{O})_{40}^-$  including the partially embedded state: (a) dipole-bound, (b) surface-bound, (c) partially embedded, (d) internally solvated electron. Reprinted with permission from ref 132. Copyright 2010 American Chemical Society.

electrons show the largest VDEs, while the partially embedded states had binding energies between those of internal and surface electrons. Warmer initial conditions are conducive to the partial solvation of the electron. Calculated VDEs for these structures are very similar to those observed for isomer I by Bowen<sup>51</sup> and Neumark,<sup>89</sup> whereas true cavity-bound structures have slightly higher detachment energies, closer to the cryogenically prepared clusters seen by von Issendorff (isomer Ib).<sup>40</sup>

Recent advances in the photoelectron spectroscopy of liquid jets have allowed for a direct test of the cluster VDE extrapolations. Bulk vertical detachment energies of 3.3–3.6 eV<sup>42,180–182</sup> for electrons in liquid water jets have been reported and are in reasonable agreement with the VDE extrapolations of isomer I clusters. In addition, the liquid jet work carried out by Siefertmann et al.<sup>42</sup> shows a second peak with a VDE of 1.6 eV. This energy agrees well with extrapolated VDEs of isomer II cluster anions, although it is worth noting that other experimental groups<sup>180–182</sup> have not seen the low VDE peak in liquid jet photoelectron spectra. These results are discussed in more detail elsewhere in this volume. The more tightly bound electrons in the liquid jets are from fully solvated electrons, consistent with assigning at least the large isomer I clusters to internally solvated structures. The correspondence between the lower VDE peak in the liquid jet and the isomer II VDEs has led to the proposal that the former is from electrons at the jet-vapor interface.<sup>42</sup>

### 3.2. Dynamics in Water-Based Cluster Anions

The time-resolved dynamics of electrons in water clusters can be addressed in two different but complementary ways. First,

probing the relaxation dynamics of electronically excited water cluster anions  $(\text{H}_2\text{O})_n^-$  allows one to determine excited state lifetimes in hydrated electron clusters, thus giving insight into how relaxation of the bulk hydrated electron proceeds. Second, the dynamics following charge-transfer from iodide in  $\text{I}^-(\text{H}_2\text{O})_n$  clusters give insight into the molecular motions associated with charge-transfer-to-solvent in solution.

The first experimental investigation into the lifetime of the excited state in water cluster anions was performed in 2001 by Johnson and Cheshnovsky using femtosecond resonant-two-photon detachment (R2PD) spectroscopy.<sup>183</sup> In these experiments, a significant two-photon detachment signal was detected using  $\sim 100$  fs, 800 nm pulses, first appearing around  $n = 30$  and increasing in intensity through  $n = 100$ , as the transition approached resonance. The lifetime of the upper state was estimated to be bounded from above by the pulse width, but no explicitly time-resolved measurements were made.

Time-resolved photoelectron imaging experiments by the Neumark group<sup>43,89,177</sup> on size selected water cluster anions out to  $n = 100$  directly probed the population dynamics and energetics of the cluster excited state. Representative time-resolved photoelectron spectra are shown for  $n = 25$  in Figure 9a using  $h\nu_{\text{pump}} = 1.0$  eV and  $h\nu_{\text{probe}} = 3.1$  eV. Schematic potential energy surfaces for  $(\text{H}_2\text{O})_n^-$  detailing the features in the photoelectron spectra are shown in Figure 9b, indicating the origin of the four features A–D seen in Figure 9a. Feature D, representing the excited state population, rises abruptly when the pump and probe pulses overlap and then decays with

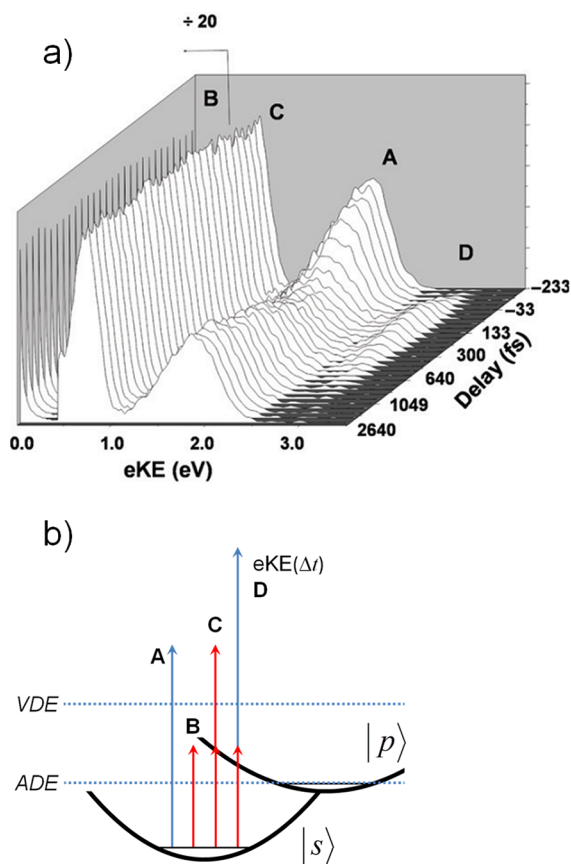


**Figure 9.** (a) Time-resolved photoelectron spectrum for  $(\text{H}_2\text{O})_{25}^-$  with  $h\nu_{\text{pump}} = 1.0$  eV and  $h\nu_{\text{probe}} = 3.1$  eV. (b) Schematic potential energy surfaces showing photoelectron spectra features.

a time constant of  $\sim 400$  fs for  $n = 25$ . Feature A, the ground state population, is initially depleted but then recovers on the same time scale at which feature D decays. These complementary dynamics are a clear signature that the cluster excited state decays by internal conversion to the ground state, and that the TRPE spectrum thus provides a direct measure of the IC lifetime. R2PD signal from the ground state is also seen (C) along with excited state autodetachment (B).<sup>177</sup>

The excited state lifetimes of isomer I decrease dramatically as the cluster size increases. Extracted lifetimes for  $(\text{H}_2\text{O})_n^-$  and  $(\text{D}_2\text{O})_n^-$  are shown in Figure 10 as a function of  $1/n$ . The most

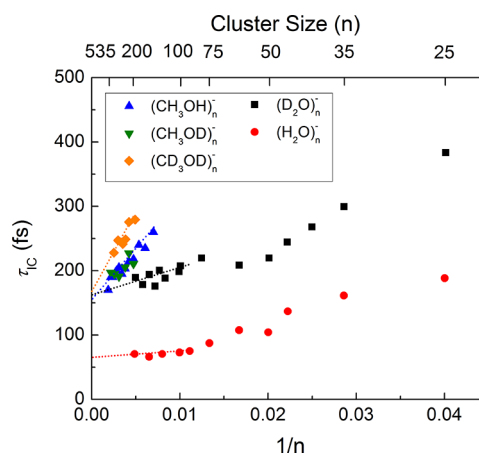


**Figure 10.** Extracted internal conversion time scales for isomer I of  $(\text{H}_2\text{O})_n^-$ ,  $(\text{D}_2\text{O})_n^-$ ,  $(\text{CH}_3\text{OH})_n^-$ ,  $(\text{CH}_3\text{OD})_n^-$ , and  $(\text{CD}_3\text{OD})_n^-$  vs  $1/n$ .

notable feature of Figure 10 is the approximately linear nature of the isomer I relaxation times beginning around  $n = 25$ . Fischer<sup>184</sup> has proposed that this  $1/n$  dependence arises from long-range nonadiabatic coupling of transition dipoles. In this framework, internal conversion is prompted by coupling between the OH stretch and  $s-p$  transition dipole moments, leading to a  $1/R^3$  ( $\propto 1/n$ ) dependence. More recent experiments with higher temporal resolution and on larger sizes<sup>185</sup> show a change in slope of the lifetimes versus  $1/n$  around  $n = 70$ . Extrapolating beyond this size yields bulk internal conversion lifetimes of  $\sim 60$  and  $\sim 160$  fs for  $\text{H}_2\text{O}$  and  $\text{D}_2\text{O}$ , respectively. The extrapolated lifetime for  $(\text{H}_2\text{O})_n^-$  clusters strongly supports the nonadiabatic model for relaxation of the bulk hydrated electron outlined in section 3.

While the first set of TRPE experiments on water cluster anions yielded excited state lifetimes only,<sup>43,177</sup> the more recent work<sup>185</sup> showed that feature D shifts toward lower eKE prior to disappearing. The shift is consistent with vibrational relaxation in the excited state into non-Franck–Condon active modes. This time-dependent shift is shown in Figure 11 for  $(\text{D}_2\text{O})_{75}^-$  along with the integrated intensity of peak D. These results are interpreted to indicate that the time scales for excited state relaxation (eq 7) and internal conversion are comparable.

Warmer isomer I clusters produced in neon expansions are found to undergo similar dynamics to those previously reported, but with even faster internal conversion lifetimes.<sup>157</sup> Lifetimes for Isomer I clusters from  $n = 25$ –40 are shorter by as much as 50 fs compared to clusters of the same size made in argon, appearing to converge with the previously measured lifetimes at larger sizes. Importantly, the extrapolated bulk lifetime is again estimated as  $\sim 60$  fs for water.

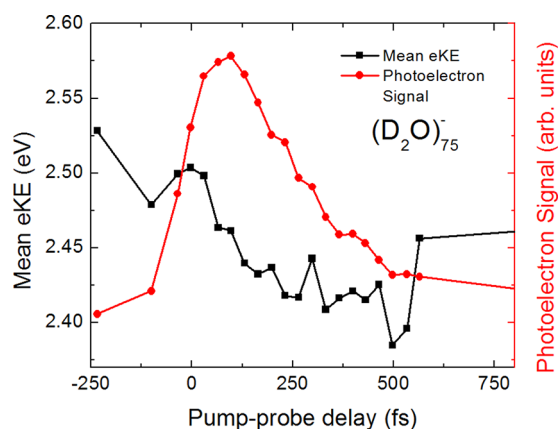


**Figure 11.**  $\langle eKE \rangle$  of feature B as a function of pump–probe delay for  $(D_2O)_{75}^-$  showing the change in the excited state spectrum indicating possible relaxation along the  $p$ -state.

Dynamics in water cluster anions were also studied by Zewail and co-workers,<sup>55</sup> who focused on the dynamics of the ground state following  $p \leftarrow s$  excitation for  $n = 15$ – $35$ . They found that following internal conversion, relaxation on the ground state occurs on a  $\sim 300$  fs time scale, irrespective of cluster size. The distribution of that energy, however, takes significantly longer, about 2–10 ps over that size range, decreasing dramatically at larger sizes. They interpreted these time scales as relaxation of the first and outer solvation layers via intramolecular vibrational redistribution.

Hertel and co-workers<sup>186</sup> monitored the ultrafast relaxation of solvated electrons in sodium doped neutral water clusters,  $Na(H_2O)_n$ , for  $n = 2$ – $40$ . Similar to the one-photon experiments by Buck,<sup>162–164</sup> the electron is spontaneously driven from the sodium atom and associates with the solvent network, resulting in a perturbed solvated electron cluster, which is then interrogated with pump–probe photofragment spectroscopy. They find that the lifetime of the excited state decreases dramatically from 1.2 ps for  $n = 2$  to around 100 fs for clusters  $n \approx 22$ , after which the lifetimes are effectively constant. Around  $n = 30$ , the lifetimes are approximately equal to those in the bare water cluster anions, possibly indicating the maximum size where the sodium ion perturbation to the solvent structure is significant.

The key result of the time-resolved experiments on clusters is the observation of the sub-100 fs internal conversion lifetimes for the largest clusters. This lifetime is in excellent agreement with the shortest time scales (30–80 fs) observed in the transient absorption experiments. Thus it appears the excited state relaxes via the nonadiabatic pathway described above. The  $\sim 60$  fs lifetime is also in good agreement with calculated internal conversion times for an electron solvated in a dielectric continuum parametrized for water.<sup>187</sup> In addition, both the  $\sim 300$  fs and  $\sim 1$  ps ground state relaxation time scales measured by the Zewail<sup>55</sup> group are consistent with the nonadiabatic relaxation mechanism. Our observation of possible relaxation along the excited surface is still consistent with this model, as the sub-100 fs internal conversion process is still faster than the other two time scales observed; the  $p$ -state relaxation is simply faster than what had previously been measured.

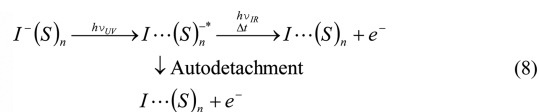
The Hertel and Neumark studies showed a very strong isotope effect for the internal conversion lifetimes, with  $\tau_D/\tau_H \sim 2.8$ – $3.6$ , and both groups interpreted this within the context of the “energy gap” law for internal conversion in which the rate is

determined primarily by Franck–Condon factors.<sup>188</sup> Because the Franck–Condon overlap is strongly dependent on the energy gap between the states, the rate of internal conversion will dramatically decrease for larger energy differences. However, this model may fail for the larger water clusters, where the short excited state lifetimes ( $<100$  fs) may be a result of a conical intersection between the potential energy surfaces. Semiclassical<sup>189</sup> and mixed quantum/classical molecular dynamics<sup>190</sup> studies find large isotope effects as well, though the magnitudes of the internal conversion lifetimes calculated are much larger than those seen experimentally in each case.

### 3.3. Dynamics in Halide–Water Clusters

A second set of cluster dynamics experiments takes advantage of the cluster analog to the well-known charge-transfer-to-solvent (CTTS) transition in liquids.<sup>147</sup> In hydrated anions such as iodide, ultraviolet excitation near the detachment energy accesses the CTTS transition, which ejects the excess electron into the solvent network, as shown in Figure 2b. The gas-phase precursors to these CTTS states were first observed in 1996 by Johnson and co-workers<sup>191</sup> in  $I^-(H_2O)_n$  clusters, where the absorption cross section peak was observed to increase from  $\sim 3.5$  eV for  $n = 1$  to  $\sim 4.5$  eV for  $n = 4$ . CTTS excitation in clusters transfers the electron to the solvent moiety near the dopant, forming a solvent cluster anion complexed with neutral iodine. The initial geometry of these clusters is reasonably well-known from infrared spectroscopy experiments and the accompanying theory.<sup>94</sup> The system just after photoexcitation can be conceptualized as an iodine–solvent cluster anion in its ground electronic state but with the solvent cluster nuclear geometry perturbed to optimally solvate the ion instead of the electron, a picture confirmed in theoretical treatments such as those performed by Peslherbe and co-workers.<sup>192,193</sup>

In a series of experiments,<sup>153,194–197</sup> Neumark and co-workers performed time-resolved photoelectron spectroscopy and imaging to follow the solvation dynamics following charge transfer from iodide in real time



In these experiments, which are the cluster analog of Figure 2b, a femtosecond UV (245–266 nm) excitation pulse pumps the CTTS transition and transfers the electron onto the cluster, while electrons were detached using an infrared (790 nm) probe. Figure 12a displays the time-resolved photoelectron spectrum of  $I^-(D_2O)_7$ , which exhibits a temporally evolving excited state (feature B) bound by only a few hundred millielectronvolts. For smaller clusters, the UV excitation energy exceeds the adiabatic detachment energy. Hence, the excited state can decay by autodetachment (eq 8), producing very slow electrons ( $<100$  meV) labeled feature A in Figure 12a. The excited state lifetimes with respect to autodetachment can be obtained by the curves shown in the inset of Figure 12a, showing the decay of feature B and recovery of feature A. The complementary dynamics indicated by the two curves confirms that autodetachment is the primary decay mechanism. The excited state lifetimes increase with cluster size from  $\sim 0.6$  ps for  $n = 3$  to  $\sim 3$  ns for  $n = 10$ , reflecting the relative stabilities of the water cluster anion states. For larger clusters,<sup>153,196</sup> autodetachment is either too slow to measure or does not occur because

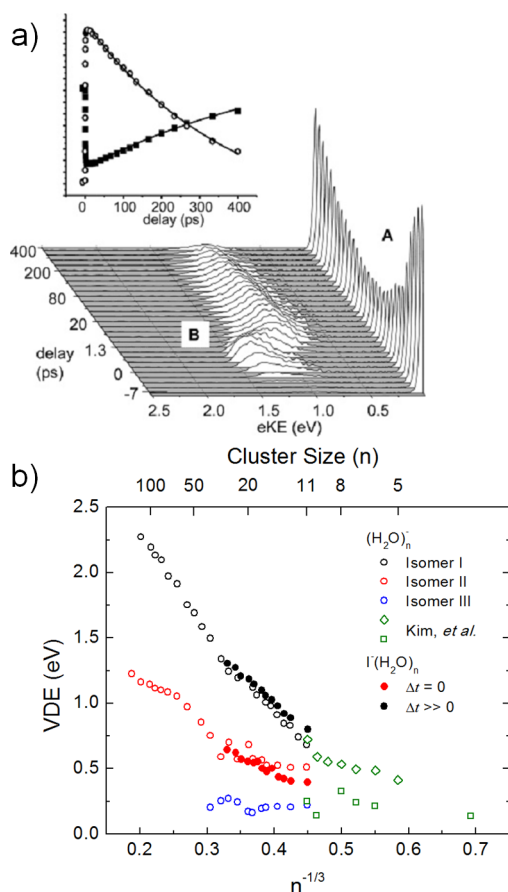


**Figure 12.** (a) Time-resolved photoelectron spectrum of  $\Gamma(\text{D}_2\text{O})_7$  with  $h\nu_{\text{pump}} = 4.71$  eV and  $h\nu_{\text{probe}} = 1.57$  eV. (b) Size dependence of early ( $t \approx 0$ , filled red circles) and late ( $\Delta t \gg 0$ , filled black circles) VDEs of  $\Gamma(\text{H}_2\text{O})_n$  following absorption in the CTTS band, along with VDEs of bare isomer I, II, and III water cluster anions.

the total internal energy of the photoexcited excited clusters is insufficient to eject an electron.

The solvation dynamics are revealed by tracking the maximum of the excited state feature and converting it to a time-dependent VDE:  $\text{VDE}(t) = h\nu_{\text{probe}} - \text{eKE}_{\text{max}}(t)$ . The VDE first rapidly ( $\sim 200$  fs) decreases by 30–400 meV before recovering to a maximum over the next 1–2 ps.<sup>196</sup> The magnitude of these changes increases with cluster size. After reaching a maximum, the VDE then falls by  $\sim 50$  meV for all cluster sizes over the next  $\sim 10$  ps. The first drop in VDE occurs rather quickly, before any significant solvent relaxation can occur. Calculations by Peslherbe<sup>193</sup> on  $\Gamma(\text{H}_2\text{O})_5$  suggest that the initial drop in VDE arises from electron and solvent dynamics from a repulsive interaction between the detached electron and nearby solvent molecules. The strong size-dependence of the second energy shift indicates that it originates from changes in the solvent structure. Indeed, solvent motions are seen in the excited state simulations by Takayanagi<sup>198,199</sup> and Kim.<sup>200</sup> Conversely, the final  $\sim 50$  meV decrease in VDE is independent of cluster size. This shift could be due to the ejection of the neutral iodine from the cluster, as iodine has been shown to stabilize water clusters by a similar amount.<sup>201</sup> As discussed above, over this size range the anionic water clusters are characterized as surface states, so with the iodide on the surface, the cluster does not have to undergo severe reorganization to accommodate the excess charge.

Theoretical treatments of these cluster dynamics have also been reported by Sheu<sup>202</sup> and Jordan.<sup>203</sup>

Comparison of the VDEs of the  $\Gamma(\text{H}_2\text{O})_n$  excited states at various pump–probe delays to those of the isomer I and II  $(\text{H}_2\text{O})_n^-$  clusters suggests that the binding motif of the electron changes significantly throughout the relaxation process. Initially following charge-transfer ( $\Delta t \approx 0$ ), the electron is only bound by a few hundred meV, similar to isomer II water cluster anions. After the relaxation dynamics are mostly complete ( $\Delta t \gg 0$ ), the VDEs have significantly increased, becoming very similar to those of isomer I clusters, as shown in Figure 12b up to  $n = 28$ .<sup>89,153</sup> It appears the clusters isomerize from the surface bound to the (partially-) internally bound electron states on few ps time scale.

It was recently observed that the excited state lifetimes in  $\Gamma(\text{H}_2\text{O})_n$  clusters are strongly dependent on the energy used to pump the CTTS transition.<sup>197</sup> The excited state lifetime of  $(\text{H}_2\text{O})_6^-$ , for example, decreases from  $\sim 160$  ps to  $\sim 75$  ps as the pump energy is increased from 4.55 to 5.06 eV. These results were interpreted within the framework of a thermionic emission model proposed by Klots,<sup>37</sup> wherein the excess energy after charge-transfer is redistributed statistically throughout the vibrational modes of the system. The relative energetics of the anion and neutral system appear to determine the autodetachment lifetime, as opposed to specific geometric or structural effects.

#### 4. METHANOL

Methanol ( $\text{CH}_3\text{OH}$ ) is chemically similar and closely related to water, though many of its properties are very different owing to the broken symmetry of the molecule. Because it only has the ability to form one hydrogen bond per molecule, the structure of bulk methanol<sup>204</sup> and methanol clusters<sup>205</sup> differs significantly from that of water and water clusters. Many studies on the solvated electron in methanol have been conducted in the bulk,<sup>26,206–210</sup> and the consensus is that, like in water, the electron resides in a quasi-spherical cavity with the OH groups directed at the electron center of mass.<sup>9,211,212</sup> From moment analysis of the electronic absorption spectrum, the cavity in methanol has a radius of 2.25–2.28 Å.<sup>133,213</sup> The relaxation dynamics of electrons in methanol have also been measured by transient absorption experiments where the excess electrons are created either by multiphoton ionization<sup>210</sup> of the solvent or by CTTS excitation.<sup>209</sup> Three-pulse experiments by Thaller et al.<sup>210</sup> show the electron is solvated through an intermediate “hot” state that thermalizes on a  $\sim 10$ –20 ps time scale. The excited state dynamics occur with 2 or 3 time scales, depending on the pump wavelength,<sup>26,208,210</sup> the fastest of which was on the order of 100–200 fs. The proposed relaxation schemes are similar to those proposed for water, with similar ambiguities regarding the time scale for internal conversion vs excited state relaxation. Photoelectron spectra of solvated electrons in liquid jets of methanol have been measured by Suzuki and co-workers,<sup>214,215</sup> with the most recent work yielding a VDE of  $3.38 \pm 0.04$  eV. Zeuch et al.<sup>216</sup> have also estimated the bulk binding energy of methanol solution by extrapolating the IPs from  $\text{Na}(\text{CH}_3\text{OH})_n$  clusters ( $n = 6$ –40) and predict the electron to be bound by 3.19 eV, close to the liquid jet value.

Clusters of neutral methanol have been studied using infrared predissociation spectroscopy,<sup>205,217</sup> neutron spectroscopy<sup>218</sup> and DFT calculations,<sup>219</sup> but the negative ions,  $(\text{CH}_3\text{OH})_n^-$  have received little attention until quite recently.<sup>220</sup> Neutral methanol clusters exist in structures

where the number of hydrogen bonds is maximized, typically with the hydroxyl groups directed inward toward the cluster center and methyl groups at the cluster surface;<sup>218</sup> this holds at the liquid–air interface for bulk methanol, as well.<sup>214</sup> The dominance of hydrophobic CH<sub>3</sub> groups at the neutral cluster surface is very different from water clusters and might be expected to favor internal vs surface solvation of an excess electron.

Photoelectron imaging experiments on methanol cluster anions produced via supersonic expansion were carried out by Neumark and co-workers in 2006.<sup>221</sup> These experiments covered a large range of cluster sizes,  $71 \leq n \leq 460$ . Similar to water cluster anions, photoelectron spectra of methanol cluster anions show evidence for two isomers over a wide size range depending on the source conditions. Photoelectron spectra of  $n = 190$  at various stagnation pressures are shown in Figure 13a, along with spectra of various cluster sizes at 20 psig

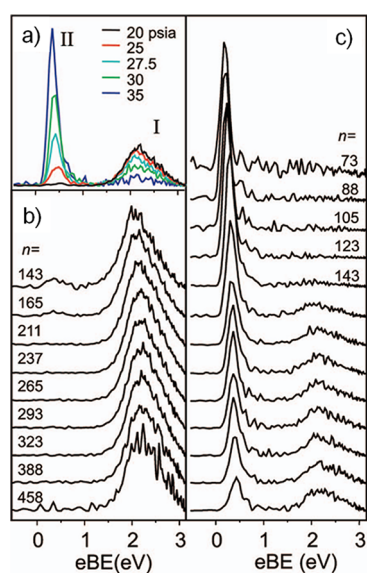


**Figure 13.** (a) Photoelectron spectra of  $(\text{CH}_3\text{OH})_{190}^-$  at various stagnation pressures. (b) Photoelectron spectra taken at 3.10 eV photon energy at 20 psig stagnation pressure. (c) Photoelectron spectra taken at 3.10 eV photon energy at 30 psig stagnation pressure. Reprinted with permission from ref 221. Copyright 2006 American Institute of Physics.

(Figure 13b) and 30 psig (Figure 13c). At lower stagnation pressures (warmer expansion conditions), large ions ( $n \approx 140$ ) are observed with binding energies above 2 eV; as in the case in water, these are designated isomer I. At higher stagnation pressures (colder expansion) a more weakly bound isomer dominates the spectrum, appearing at  $n \approx 70$  with VDEs around 0.3–0.5 eV; these are labeled isomer II. Isomers I and II were assigned to internal and surface bound electrons, respectively. The isomer II photoelectron spectra are fairly narrow, only  $\sim 150$  meV, suggesting similar anion and neutral geometries. Extrapolation of the cluster VDEs to infinite size yields 2.51 eV for isomer I and 0.74 eV for isomer II, with slopes of  $-2.25$  and  $2.41$  eV, respectively, as seen in Figure 4.

The existence of two different binding motifs was recently seen in mixed quantum/classical molecular dynamics simulations by Turi and co-workers,<sup>124,131</sup> using a newly developed electron-methanol pseudopotential.<sup>222</sup> This work showed that the electron can be associated either with the hydroxyl groups

at the center of the cluster or with the methyl-rich surface through collective polarization interactions. Several key properties of methanol cluster anions are recovered in the simulations which support the assignments proposed in the photoelectron study. Specifically, the two states have vastly different binding energies. For example, the internally bound electron for the  $n = 512$  cluster is bound by  $\sim 2.9$  eV while the surface state is only bound by 0.75 eV. The surface states are diffuse with large radii of gyration (8–10 Å), which is consistent with the lower binding energies and narrow photoelectron spectra of isomer II. Internal solvation is only seen for larger sizes ( $n > 128$ ), similar to the delayed onset of isomer I states in the clusters ( $n > 140$ ) in the study by Neumark.<sup>221</sup> Linear evolution of the binding energy with  $n^{-1/3}$  is also seen in the simulations allowing for comparison to the bulk binding energy. Indeed, extrapolating Turi's work (200 K) internally bound and surface bound electron binding energies yields bulk estimates of  $\sim 3.5$  and 1.1 eV, respectively. The bulk estimate for the internally bound state is also higher than that from simulations of the electron in liquid methanol, about 2.4 eV at 200 K, likely due to the neglect of long-range interactions.<sup>131</sup>

The relative stability of the two states is revealed in the solvation dynamics for differently prepared initial electron distributions and for different sizes, as explored by Mones et al.<sup>131</sup> An electron initially launched from the cluster interior diffuses toward the surface in smaller sizes ( $n < 128$ ), while in larger systems it remains internally localized. On the other hand, when the electron is placed at the cluster surface at the beginning of the simulation, it tends to remain on the interface, maintaining its large radius of gyration in smaller systems. However, solvation of an initially surface-bound electron does occur in larger clusters at 200 K, as the wave function penetrates into the cluster and contracts, resulting in a larger binding energy. Snapshots of the electron solvation process are shown in Figure 14.

Additional insight into the influences of the molecular environment on solvated electron clusters can be gained from investigating the excited state dynamics of  $(\text{CH}_3\text{OH})_n^-$ . Large methanol cluster anions support a bound excited state near 1.55 eV, as evidenced by an R2PD feature at that energy.<sup>221</sup> Just as in water, this state is similarly red-shifted in the clusters relative to liquid methanol, as the solvated electron in bulk methanol has its absorption maximum at 1.95 eV (635 nm).<sup>223</sup> Turi and co-workers also show this state for clusters between  $n = 161$  and  $n = 500$ , peaking around 2.2–2.3 eV, slightly blue-shifted from the bulk value, likely because of the lack of excited-state polarization in the simulations.<sup>131,222</sup>

As with water cluster anions, time-resolved photoelectron imaging experiments were carried out on isomer I of  $(\text{MeOH})_n^-$  ( $n \approx 145$ –535) by the Neumark group.<sup>224</sup> The time-resolved experiments monitor both the ground and excited state populations and energetics and show clear internal conversion on a  $\sim 180$ –270 fs time scale over this size range. Similar to  $(\text{H}_2\text{O})_n^-$ , the excited state lifetimes are linear with  $1/n$ , as shown in Figure 10, possibly due to the same dipolar coupling proposed by Fischer,<sup>184</sup> but the lifetimes are significantly longer than in corresponding water clusters. Extrapolation to infinite cluster size yields a bulk internal conversion lifetime of 157 fs, again in agreement with fastest reported time scales from transient absorption experiments,<sup>208,210</sup> and suggesting that the “non-adiabatic” relaxation mechanism proposed for electrons in water<sup>28</sup> also applies to methanol. This lifetime is also in remarkable agreement with

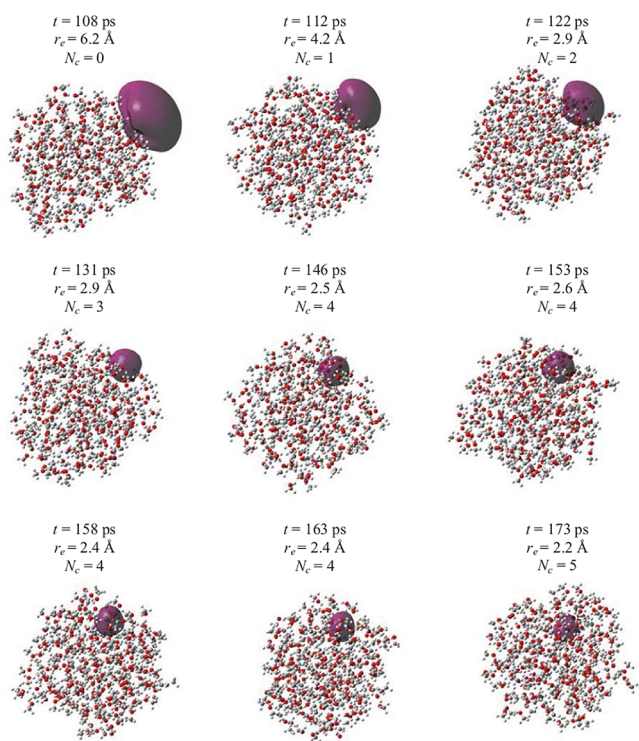


**Figure 14.** Mechanism for electron solvation in methanol clusters for  $(\text{CH}_3\text{OH})_{205}^-$  at  $T = 200$  K as a function of time. The electronic isosurface represents 80% of the excess electron density. The radius of gyration ( $r_g$ ) and electron-solvent coordination number ( $N_c$ ) are also represented. Reprinted with permission from ref 131. Copyright 2011 American Institute of Physics.

the predicted value of 150 fs from the same dielectric solvation model used with water.<sup>187</sup> Interestingly, the internal conversion lifetimes show a much less pronounced isotope effect ( $\tau_D/\tau_H \approx 1.1$  for  $\text{CD}_3\text{OD}$  and  $\text{CH}_3\text{OD}$ , see Figure.10), suggesting that the OH stretching modes do not necessarily dominate the internal conversion process, and that other modes can nonadiabatically couple to the transition. Indeed, Turi and co-workers<sup>225</sup> have demonstrated a significant nonadiabatic coupling of the OH bending, CO stretching and  $\text{CH}_3$  deformation modes to the internal conversion process. For water, where there are only OH modes, the coupling of the higher frequency vibrations may explain the faster relaxation rate and larger isotope effect relative to methanol.

The recently measured photoelectron binding energy in liquid methanol highlights an interesting discrepancy with the cluster data. Liquid jet measurements place the bulk vertical binding energy at 3.4 eV,<sup>215</sup> Turi's cluster simulations estimate it to be 3.5 eV,<sup>131</sup> and extrapolations from  $\text{Na}(\text{CH}_3\text{OH})_n$  clusters predict  $\sim 3.2$  eV.<sup>164</sup> However, the projection from the  $(\text{CH}_3\text{OH})_n^-$  isomer I clusters is significantly smaller at  $\sim 2.5$  eV. Both Turi and Zeuch attribute the higher binding energy to the uncertainty in the experimental cluster temperature.<sup>131,164</sup> Somewhat better agreement between the extrapolated binding energies of the simulated surface states and experimental isomer II clusters is seen, 1.1 and 0.7 eV, respectively. The slopes of the VDE vs  $n^{-1/3}$  plot can be estimated from dielectric continuum theory with temperature-sensitive parameters. The predicted slope decreases significantly in magnitude from  $-4.30$  to  $-2.59$  eV when solid parameters are used instead of those for the liquid, in much better agreement with the

experimentally determined slope of  $-2.25$  eV. Isomer II has a similar slope of  $-2.41$  eV.<sup>90</sup> These comparisons suggest that the methanol clusters in the anion experiments may be solid aggregates, though this is seemingly at odds with the agreement of the internal conversion time scales in the clusters<sup>224</sup> with those measured in liquid methanol.<sup>210</sup> Studies on thermally controlled clusters would greatly aid in resolving this discrepancy.

Complementary information on electron attachment and solvation can be monitored experimentally by performing time-resolved experiments on  $\Gamma(\text{CH}_3\text{OH})_n$  clusters. For small methanol clusters, halide ions such as iodide bind to the cluster surface by disrupting the hydrogen bond network and forming multiple  $\text{OH}\cdots\text{I}^-$  bonds.<sup>226–229</sup> As with water clusters, the electron can be transferred to the cluster surface by CTTS excitation and the ensuing solvation dynamics monitored with TRPEI, in this case for cluster sizes up to  $n = 11$ .<sup>197,230,231</sup> A representative time-resolved photoelectron spectrum of  $\Gamma(\text{CH}_3\text{OH})_7$  is shown in Figure 15a.<sup>231</sup>

The  $\Gamma(\text{CH}_3\text{OH})_n$  time-resolved spectra show significant differences compared to those in the  $\Gamma(\text{H}_2\text{O})_n$  experiments. The lifetimes of the nascent methanol clusters are considerably

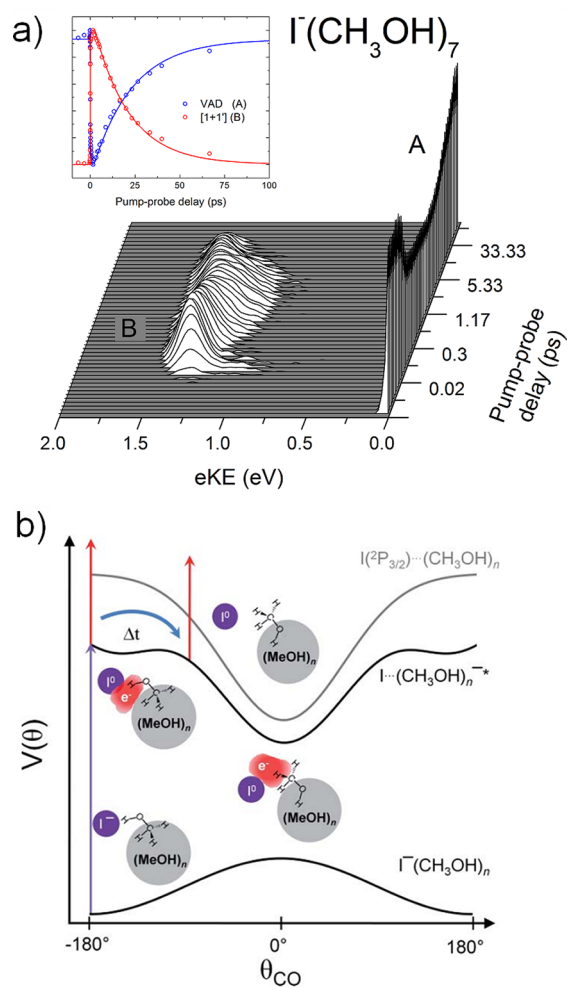


**Figure 15.** (a) Time-resolved photoelectron spectrum for  $\Gamma(\text{CH}_3\text{OH})_7$  with  $h\nu_{\text{pump}} = 4.71$  eV and  $h\nu_{\text{probe}} = 1.57$  eV. (b) Schematic potential energy surfaces of the anion ground, anion excited, and neutral states as a function of the angle of the rotating methanol CO bond and the cluster center.

shorter, only  $\sim 1$ – $80$  ps over this size range for  $h\nu_{\text{pump}} = 4.71$  eV, compared to  $300$  ps and  $3$  ns for  $\Gamma(\text{H}_2\text{O})_7$  and  $\Gamma(\text{H}_2\text{O})_{10}$  at the same energy.<sup>196</sup> They are however, similar to those observed in  $\Gamma(\text{NH}_3)_n$  clusters.<sup>232</sup> While water cluster anions are adiabatically stable over this size range, methanol and ammonia cluster anions are not.<sup>46,221</sup> Moreover, the autodetachment channel is always present, indicating the methanol cluster anions are adiabatically unbound over this size range, and the asymptotic (long pump–probe delay) vertical detachment energies in these experiments are also small, only  $80$ – $320$  meV. As with iodide–water clusters, the photon energy of the pump pulse has a significant effect on this lifetime, dropping by a factor of  $\sim 2.5$  as the photon energy is increased from  $4.71$  to  $5.21$  eV for  $n = 8$ .<sup>197</sup> The (very) low binding energy of the electron to the methanol cluster results in a short autodetachment lifetime, as the excess energy is distributed among the vibrational modes, which can then drive the electron emission process.

The dynamics subsequent to photoexcitation can be inferred from analysis of the excited state feature in the spectrum. For  $n = 4$ – $11$ , the VDE drops significantly over the first  $\sim 400$  fs before rising by as much as  $160$  meV over the next  $1$ – $2$  ps. Then, over the remainder of excited state lifetime, the VDE falls again by  $60$ – $180$  meV, indicating a destabilization relative to the neutral over a characteristic  $10$ – $20$  ps time scale.<sup>231</sup> In contrast to  $\Gamma(\text{H}_2\text{O})_n$  clusters, the changes in vertical detachment energy at long times are all strongly size-dependent, and thus are due to solvent reorganization. As the initial  $\Gamma(\text{CH}_3\text{OH})_n$  cluster geometry is significantly different than the neutral and vertically excited anion clusters owing to the reorientation of (at least one) methanol about the iodide, it is expected that this motion should drive the dynamics. Indeed, the  $10$ – $20$  ps time scale is consistent with the end-over-end rotation (half-period) of free methanol, such that the reorientation of this methanol molecule drives the electron solvation as the hydrogen bond network is re-established. The involvement of this rotational mode was also invoked in the relaxation process of hot ground state solvated electrons in liquid methanol, resulting in relaxation on a similar time scale.<sup>206–208,210</sup>

The  $\Gamma(\text{CH}_3\text{OH})_n$  photoelectron measurements<sup>231</sup> coincided with the independent study by Turi on  $(\text{CH}_3\text{OH})_n^-$  clusters.<sup>131</sup> Both groups concluded that the methanol rotation and the  $\text{OH}\cdots\text{e}^-$  interaction play central roles in the solvation process, despite the obvious differences in size and manner of electron attachment. The final fate and the degree of the perturbation by the remaining neutral iodine is unclear in these experiments, especially because of the reduced lifetime of the methanol cluster anion formed after charge transfer. An idealized schematic of the relevant potential energy surfaces for the halide–methanol clusters is shown in Figure 15b.

## 5. AMMONIA

The solvated electron was first detected in ammonia/metal solutions owing to its strong infrared absorption with a broad tail extending into the UV that gives rise to the characteristic blue color first observed by Weyl.<sup>6,17</sup> Like in water, the electron in ammonia is thought to occupy a cavity composed of  $\sim 6$  ammonia molecules, on average.<sup>17</sup> Photoemission of dilute solutions of alkali<sup>233</sup> and transition metals<sup>234,235</sup> in ammonia yields an electron binding energy of  $1.27$  eV, while studies on more concentrated solutions yield a higher estimate of  $1.45$  eV;<sup>236,237</sup> both values are significantly reduced compared to

water. Femtosecond transient absorption experiments by Vohringer and co-workers<sup>17</sup> have shown that following IR absorption, the excited state of the electron decays on a sub- $100$  fs time scale, while the absorption spectrum dynamically evolves on a slightly longer ( $150$  fs) time scale. These results were interpreted using a temperature-jump model where the spectral dynamics arise from cooling of the ground state after internal conversion, as well as with an equivalent expansion and contraction of the solvent cavity on the observed time scales.

The cluster analog of the ammoniated electron is thus of interest, as the solvent is clearly capable of stably trapping an electron while the ammonia molecule is not. Mass-spectrometric studies on  $(\text{NH}_3)_n^-$  by Haberland<sup>238,239</sup> suggest that it takes as many as  $35$  ammonia molecules to collectively bind an electron. Interestingly, perdeuterated clusters  $(\text{ND}_3)_n^-$  require  $41$  cluster units for the anion to be stable. The shape of the mass spectrum also differs upon deuteration. Kondow and co-workers<sup>240</sup> observed similar mass spectra, though with slightly different onsets of anion stabilization ( $n = 37$  for  $\text{NH}_3$  and  $n = 43$  for  $\text{ND}_3$ ). They attribute the isotopic difference to the effect of deuteration on the electron capture cross section due to the coupling of the electron motion to that of the surface hydrogen/deuterium atoms.<sup>241</sup> In 2008, Zewail and co-workers<sup>242</sup> produced  $(\text{NH}_3)_n^-$  clusters as small as  $n = 13$  using a high-pressure pulsed Even-Lavie valve well-known for producing cold molecular clusters,<sup>54</sup> indicating that enthalpy of vaporization is fairly low.

Bowen and co-workers<sup>46</sup> measured photoelectron spectra of  $(\text{NH}_3)_n^-$  ( $41 \leq n \leq 1100$ ) and compared their results to both bulk measurements of ammoniated electrons and a dielectric model. Their spectra show the same characteristic broad, featureless structure common to solvated electron PE spectra, with little variation in shape. Photoelectron spectra of the smaller clusters produced by Zewail show more structure than the larger sizes observed by Bowen, owing either to different structural isomers<sup>242</sup> or to vibrationally resolved peaks similar to those seen in smaller water clusters.<sup>89,155</sup> Ammonia clusters were shown to bind the excess electron by  $0.32$  to  $1.05$  eV over the entire range studied by both groups.<sup>46,242</sup> Plotting both sets of VDEs versus the cluster radius ( $n^{-1/3}$ ), as shown in Figure 4, yields a slope of  $-2.41$  eV with an intercept (bulk photoelectron threshold) of  $1.25$  eV. The measured binding energy of the electron in bulk ammonia, as mentioned above, is  $1.27$  eV,<sup>236,237</sup> in good agreement with the cluster data. Alkali-doped ammonia clusters have also been studied by Hertel, Fuke, and co-workers,<sup>160,161,243,244</sup> but in contrast to water, ionization potentials showed a smooth evolution toward the large  $(\text{NH}_3)_n$  IPs measured by Buck.<sup>245</sup>

Zewail and co-workers<sup>242</sup> investigated the excited state of ammonia cluster anions using time-resolved photoelectron spectroscopy with a magnetic bottle spectrometer. Specifically, they monitored the dynamics on the ground state following internal conversion of the excited excess electron in  $(\text{NH}_3)_n^-$  ( $n = 20$ – $60$ ). The  $p \leftarrow s$  transition was excited using an  $840$  nm pulse and photoelectrons were detached with a UV probe. An excited state feature was observed (but not reported) at higher kinetic energies, which then decays on a  $\sim 150$  fs time scale for this size range. As in their previous experiments with water clusters,<sup>55</sup> they attribute this decay to the internal conversion lifetime, which compares favorably to the  $\sim 50$  fs time scale measured for the electron in liquid ammonia.<sup>17</sup> Difference spectra were obtained by subtracting the long-time delay photoelectron spectrum at each measured delay, allowing for

detailed analysis of the ground state relaxation dynamics after the electron undergoes internal conversion. In these difference spectra, two features were observed: a relatively strong increase in signal near the peak of the ground state feature, and a weaker bleach on the high  $eKE$  side. Both of these features decay within  $\sim 500$  fs. The integrated intensity of the increase feature shows a strongly damped oscillation with a period of 1.6 ps. The integrated intensities of the ground state depletion feature for  $n = 20$  and  $n = 50$  are shown in Figure 16.

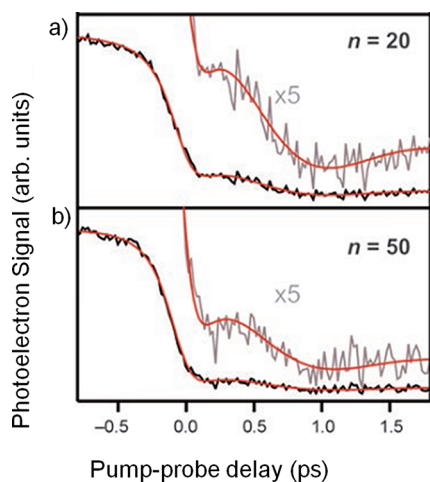


**Figure 16.** Integrated intensity of the  $(\text{NH}_3)_n^-$  transient depletion features vs pump-probe delay: (a)  $n = 20$  and (b)  $n = 50$ . Adapted with permission from ref 242. Copyright 2006, John Wiley & Sons.

Path-integral Monte Carlo simulations by Klein and co-workers<sup>128</sup> on  $(\text{NH}_3)_n^-$  suggest that the smallest clusters bind the electrons at the surface, while intermediate clusters could also support a metastable internalized state prior to decay. No coexistence of multiple binding motifs was observed in the photoelectron spectra, however the source conditions were not sampled in ways that led to the discovery of other isomers in water<sup>89</sup> and methanol.<sup>221</sup> Bennemann and co-workers<sup>106</sup> found that collective polarization of the molecular dipoles leads to stable anionic clusters after about 30  $\text{NH}_3$  molecules, while other computational studies on larger clusters by Jortner and co-workers<sup>172,246</sup> found that stable internal states exist for clusters larger than  $n = 32$ , close to the experimentally observed onset at  $n = 35$ . These studies indicate that the temperature of the cluster affects the stability of the anion, perhaps suggesting that liquid ammonia clusters are incapable of stabilizing the excess charge. A continuum polaron model proposed by Lakhno and co-workers<sup>247</sup> also reproduces the critical cluster size of  $n = 35$ , while metastable structures are predicted for  $21 \leq n \leq 35$ .

That cluster anions of  $\sim 20$ – $30$  ammonia molecules are metastable is consistent with the mass spectrometry and photoelectron spectroscopy experiments, where only clusters produced in cold conditions were observed in that size range. However, the experiments on colder clusters produced by Zewail<sup>242</sup> suggest that if these structures are metastable, they could have significant lifetimes. The smallest observed clusters could also, however, arise from fragmentation of the larger more energetic clusters as they cool in the (collisionless) molecular beam.

The notion that the clusters produced in the adiabatic expansion are cold and solid-like is consistent with several

observations made on  $(\text{NH}_3)_n^-$ . First, the slopes of the VDEs vs inverse cluster radius do not agree well with those calculated using eq 6 using liquid ammonia parameters.<sup>248</sup> However, much better agreement is achieved when the dielectric constants and density of solid ammonia are used.<sup>249</sup> Interestingly, the cluster VDEs extrapolate to the bulk liquid electron binding energy, which could indicate that the electron's radius of gyration does not change much between the liquid and solid states or that the slopes are not sensitive to the thermodynamic phase of the cluster. Second, Zewail and co-workers propose that the ground state relaxation in their time-resolved experiments is governed by more phonon-like vibrations than librations, consistent with a solid cluster environment. The damped oscillation seen in the difference spectra suggests that a coherent superposition of states is oscillating on the ground state potential energy surface after internal conversion and the degree of coherence is suggestive of a rigid solvation environment.<sup>250</sup>

The nature of the smaller ammonia cluster anions and the electron solvation process was elucidated by time-resolved photoelectron spectroscopy experiments on the charge-transfer states in  $\text{I}^-(\text{NH}_3)_n$  clusters ( $n = 4$ – $15$ ).<sup>232</sup> The excited states of these clusters are unstable with respect to electron autodetachment, though this channel was not directly observed because of the low transmission of slow electrons in the magnetic bottle spectrometer used in these experiments. As seen in iodide-doped methanol clusters, the lifetime of the  $\text{I}\cdots(\text{NH}_3)_n^*$  state is very short, only as large as 50 ps for  $n = 15$ , owing to the instability of the  $(\text{NH}_3)_n^-$  clusters at this size range.

The VDEs of the excited  $\text{I}^-(\text{NH}_3)_n$  clusters shift by as much as 200 meV for  $n = 15$  over the first 3 ps, indicating stabilization of the excess charge over time. The spectra also broaden slightly by  $\sim 20$ – $50$  meV within 1 ps, after which they remain constant, suggesting the majority of the nuclear motion is complete by that time. That any increase in the VDE is observed at all suggests that the nuclear configuration of the solvent cluster around the iodide is not optimal for the excess electron. The long-time VDEs also agree well with the calculated binding energies for the weakly bound surface states predicted to exist at this size range.<sup>128</sup> Unlike in water, where some clusters can support both an internally- and a surface-bound electron, in ammonia clusters there is no internal state at this size to allow for internalization, so only partial solvation can occur prior to autodetachment.

## 6. ACETONITRILE AND PRIMARY AMIDES

Acetonitrile ( $\text{CH}_3\text{CN}$ ) has generated significant interest due to its ability to bind excess electrons in two distinct ways simultaneously. This attribute has been known since the pulse radiolysis experiments by Bell, Rogers, and Burrows<sup>251</sup> in 1977 where two peaks were attributed to solvated monomer and dimer anions. As was shown by Kohler<sup>252</sup> and Shkrob<sup>253</sup> independently in 2002 using two very different methods, the two species are better assigned to a traditional solvated electron residing in a cavity and a dimer anion. The dimer is highly distorted with respect to the nuclear configuration of two separate  $\text{CH}_3\text{CN}$  molecules: two acetonitrile molecules are aligned in an antiparallel arrangement with a  $\sim 120^\circ$  CCN bond angle.<sup>252–256</sup> The two units share an excess electron between the low-lying  $\pi^*$  orbitals, creating a pseudocovalent bond across the alpha carbons with a bond order of about 0.6.<sup>255</sup> In the gas phase, the situation is complicated by the ability of acetonitrile and its smaller clusters to bind an excess electron via the

charge-dipolar interaction, owing to the high polarity of the  $\text{CH}_3\text{CN}$  molecule (3.92 D).<sup>257–259</sup> Calculated structures for the three different species are shown in Figure 17.<sup>254</sup>

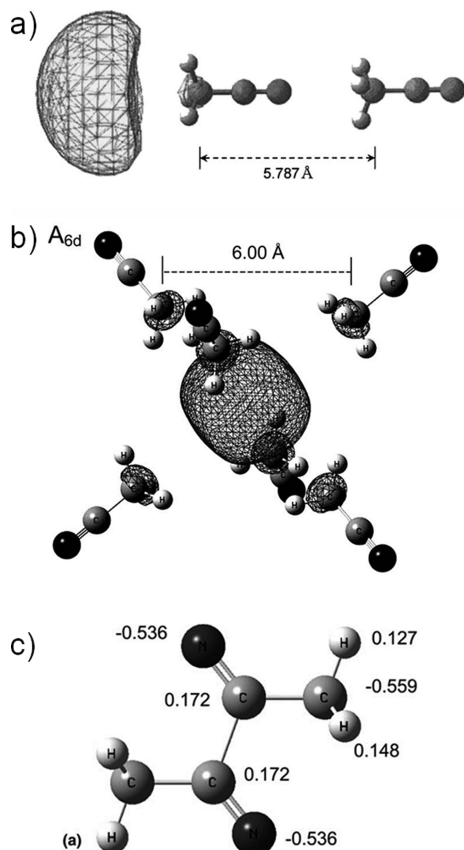


**Figure 17.** Different binding motifs of an excess electron in acetonitrile clusters. (a) Dipole-bound anion for  $(\text{CH}_3\text{CN})_2^-$  in a head-to-tail arrangement. Reprinted with permission from ref 254. Copyright 2005 American Institute of Physics. (b) Solvated electron structure for  $(\text{CH}_3\text{CN})_6^-$  showing the octahedral solvent cavity (isomer I). (c) Valence bound dimer anion; this anion becomes solvated and lies at the core of isomer II. Panels b and c reprinted from ref 260 with permission. Copyright 2006 Elsevier.

Negative ions of acetonitrile clusters  $(\text{CH}_3\text{CN})_n^-$  ( $10 \leq n \leq 100$ ) were first observed and characterized by Kaya and co-workers using photoelectron spectroscopy.<sup>76</sup> Their spectra showed that these clusters, like the bulk liquid, exhibit the coexistence of two distinct binding motifs for an excess electron with the relative populations of each state evolving with cluster size. Representative photoelectron spectra are shown in Figure 18a. The more weakly bound isomer (isomer I) appears over the entire size range and has a binding energy of  $\sim 0.4$ – $1.0$  eV. The second species (isomer II) is seen at slightly larger sizes and is bound by  $\sim 2.2$ – $2.8$  eV over the size range studied. Acetonitrile isomer II appears with very low intensity at  $n = 11$ , but quickly grows to be the dominant feature in the kinetic energy spectra, becoming nearly equal in intensity to isomer I by  $n = 12$ . By  $n = 30$ , the signal from isomer II dwarfs that from isomer I, though the latter is still present and persists out to  $n = 100$ . The hole-burning spectra in Figure 18b clearly show two independent isomers and link each to its bulk counterpart on the basis of its photodetachment cross section. Because this cross section depends on the kinetic energy of the free electron,

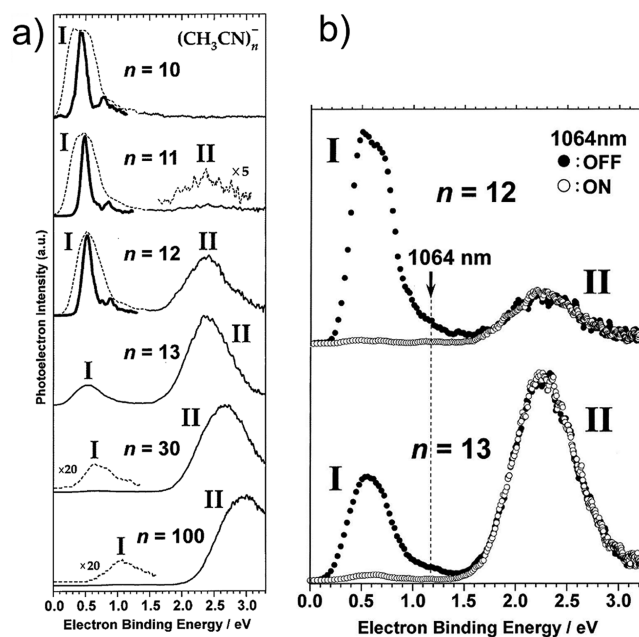


**Figure 18.** (a) Photoelectron spectra of  $(\text{CH}_3\text{CN})_n^-$  taken with 3.496 eV photon energy at 100 psig stagnation pressure. Coexistence of isomers I and II appears at  $n = 11$ , after which isomer II rapidly dominates the spectra. 18b: Hole-burning photoelectron spectrum of  $n = 12$  and  $n = 13$ . Application of 1064 nm photons detaches isomer I but leaves the isomer II population intact, suggesting they are different, unrelated species. Reprinted with permission from ref 76. Copyright 2003 American Physical Society.

the signal from a more diffuse electron will decrease with increasing photon energy as the overlap diminishes due to the higher node density in the corresponding free-electron wave function; the reverse is true for a localized electronic state. As seen in Figure 18b, isomer I appears to bind the excess electron in a diffuse molecular orbital such as a dipole-bound or solvated electron cluster state, while isomer II is a more localized state, as is expected for the dimer anion.

Much computational effort has been devoted to understanding the nature of each anion state and its behavior with cluster size. Takayanagi<sup>254</sup> employed density functional theory to investigate how small clusters ( $n = 2$ – $10$ ) bind the electrons and the effect of solvation. Two stable and distinct isomers were also observed, with VDEs separated by several electronvolts. The dimer anion was again found in the same geometry, but it was determined to be unstable with respect to electron autodetachment until solvation by two additional  $\text{CH}_3\text{CN}$  molecules. An internally bound electron structure was also seen for the geometry-optimized  $n = 6$  cluster but not for larger sizes. The structure is shown in Figure 17b. In a separate study,<sup>260</sup> the internally solvated state was observed along with the dipole-bound state for  $n = 2$  and 3. Dipole-bound states were observed for  $n = 2$  and 3 but only bind the electron by  $\sim 4$ – $150$  meV owing to the increasingly large dipole moments of these clusters. The symmetric dimer and trimer clusters can also solvate an electron internally, and despite their low net dipole moments, these anions have binding energies of several hundred millielectronvolts. The higher stability of the solvated electron species compared to the dipole-bound state, along with the decreased entropy associated with a linear head-to-tail geometry suggest that the dipole-bound species is not prevalent at larger sizes.

The association of the two gas phase isomers with their bulk counterparts is supported by time-resolved photoelectron imaging studies by Neumark and co-workers<sup>91</sup> in which the presence of a metastable excited state of isomer II was found near the bulk absorption maximum for the dimer anion in clusters of  $n = 20$ – $50$ . The excited clusters undergo vibrational autodetachment upon excitation at 800 nm, which is red-shifted from the transition in the bulk as expected for smaller aggregates. This peak was only observable because photoelectron imaging is sensitive to low-energy electrons. The excited state lifetime of these clusters was determined to be  $\sim 200$ – $300$  fs, showing no clear size dependence. Photoelectron angular distributions also support the isomer assignments qualitatively, as direct detachment from isomer I was asymmetric, with  $\beta_2 \approx 0.60$ , indicating the molecular orbital has significant spherical symmetry. Detachment from isomer II gave lower anisotropy values ( $\beta_2 \approx 0.35$ ), suggesting the HOMO undergoes more  $s$ – $p$  mixing than for isomer I, as would be expected with the pseudocovalent bond in the dimer anion.<sup>255</sup>

Neumark and co-workers also investigated electron solvation after CTTS excitation of  $\Gamma(\text{CH}_3\text{CN})_n$  ( $n = 5$ – $10$ ).<sup>261</sup> These clusters represent an interesting counterpoint to the  $\Gamma(\text{H}_2\text{O})_n$  system, for which the iodide ion is generally regarded to be located at the water cluster surface.<sup>262</sup> Similar to the excess electron in  $(\text{CH}_3\text{CN})_n^-$  isomer I, iodide is thought to be internally solvated within the cluster. Photoelectron experiments on  $\Gamma(\text{CH}_3\text{CN})_n$  out to  $n = 55$  by Cheshnovsky and co-workers<sup>263</sup> show that the solvent stabilization energy for  $\Gamma(\text{CH}_3\text{CN})_n$  levels out significantly around  $n = 12$ , indicating a closure of the first solvation shell. They find good agreement between their VDEs and calculated (classical) electrostatic stabilization energies for cluster structures with the iodide at the center with the  $\text{CH}_3$  groups directed toward it. Although the solvation shell is not closed in the size range considered by Neumark, iodide is still expected to be internally solvated based on calculations by Takayanagi.<sup>264</sup>

Following UV excitation of the CTTS band, the VDE is observed to drop over the first 300–400 fs, then rise biexponentially on 1–2 ps and 100–150 ps time scales. The excited clusters can decay by autodetachment, as  $(\text{CH}_3\text{CN})_n^-$  isomer I clusters are not adiabatically stable until  $n = 10$ .<sup>76</sup> However, the excited state lifetimes are rather long, as the autodetachment signal does not recover and the excited state signal does not decay over the experimental window of 200 ps. Given these long lifetimes, the asymptotic (long-time) VDEs can give an estimate of the binding energies of the nascent  $(\text{CH}_3\text{CN})_n^-$  clusters. These binding energies increase with cluster size and extrapolate reasonably to the binding energies for  $n = 10$ – $12$  observed by Kaya,<sup>76</sup> suggesting that the final state of these experiments is an internally bound electron. The changes in the VDEs are interpreted as arising from the electron being ejected from the internally solvated iodide to a diffuse state inside the solvent cavity, and the subsequent solvent motions necessary to stabilize the electron within the cluster. The iodine is either ejected from the cluster or weakly perturbs the system. Indeed, simulations by Takayanagi<sup>264</sup> showed that photoexcitation of smaller  $\Gamma(\text{CH}_3\text{CN})_n$  clusters causes the charge to transfer to within the cavity, which then contracts as the iodine is driven out of the cluster within the first 800 fs, leaving  $\text{I} + (\text{CH}_3\text{CN})_n^-$ . The  $\sim 1$ – $2$  ps rise-time of the VDE is interpreted as the time scale of the solvent reorganization, while the longer 100–150 ps decrease is likely

due to evaporation of either a  $\text{CH}_3\text{CN}$  monomer or the neutral iodine, both of which stabilize the cluster by about the same energy ( $\sim 50$  meV).<sup>76,196</sup>

Takayanagi has also studied the dynamics of electron attachment to small  $\text{CH}_3\text{CN}$  clusters using mixed quantum-classical MD simulations<sup>265</sup> for clusters as large as  $n = 100$ . He finds that the electron initially associates with the shallow potential local minima on the cluster surface before it is stabilized by solvent motions over the next  $\sim 10$  ps, at which point the electron is stably internally solvated. Accordingly, internalization is favorable over surface solvation for all cluster sizes of this solvent in this study, except at very low temperatures ( $\sim 5$  K).

Motivated by the identification of the quasi-bound dimer anion excited state, Head-Gordon and co-workers<sup>256</sup> have recently investigated its nature and the mechanism for excited-state autodetachment. The relevant potential energy surfaces are shown schematically in Figure 19. In support of previous

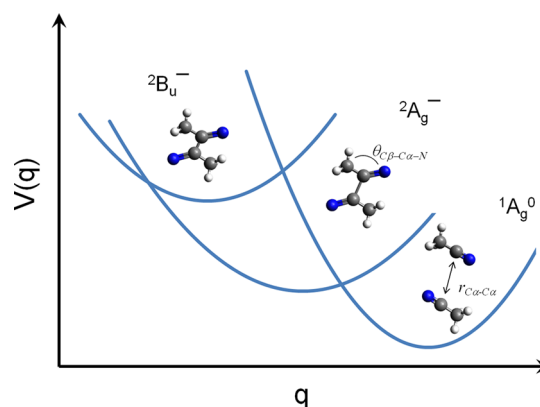


**Figure 19.** Schematic potential energy surfaces for the acetonitrile dimer anion excited state (left), ground state (middle), and neutral, antiparallel configurations (right). Adapted from ref 256.

studies, they find the most stable way to bind an excess electron is through the valence-bound dimer anion, the  $^2A_g^-$  state in Figure 19. They also identified a quasi-bound  $^2B_u^-$  excited state about 2 eV above the ground state. Their calculations show that solvation lowers the excitation energy to 1.63 eV, near the experimentally measured value of 1.57 eV. Presumably this band is broad, since in the experiments the same frequency was used to excite a wide cluster size range ( $n = 20$ – $50$ ) while the laser bandwidth itself was around 50 meV.<sup>91</sup> The anion excited state minimum energy structure is only slightly different from that of the ground state: the  $\alpha\text{C}$  distance is shorter and the CCN bond angle is further distorted by  $\sim 7^\circ$ . Considering these geometries and that of the neutral  $^1A_g^0$  state (two antiparallel  $\text{CH}_3\text{CN}$  molecules), the important normal modes for autodetachment appear to be the  $\alpha\text{C}$  distance and the CCN bond angles. Assuming only motion along these coordinates, an autodetachment lifetime was calculated. Vertical excitation to this state from the dimer anion ground state with 1.57 eV generates a wavepacket on the excited surface with the largest contribution from the  $\nu = 5$  vibrational state. The autodetachment lifetimes can then be estimated as the product of the dissociative mode frequency and the integrated probability density of the  $\nu = 5$  state beyond the  $^2B_u^-$ – $^1A_g^0$  seam. These lifetimes are approximately  $\sim 430$  fs, in good agreement with the measured values<sup>91</sup> of 200–300 fs.

Cluster anions composed of primary amides such as formamide ( $\text{CHONH}_2$ ), acetamide ( $\text{CH}_3\text{CONH}_2$ ), and propionamide ( $\text{C}_2\text{H}_5\text{CONH}_2$ ), also exhibit two coexisting binding motifs similar to those in acetonitrile cluster anions. Maeyama et al.<sup>77,78</sup> investigated these species using a magnetic bottle photoelectron spectrometer and in each case observed cluster anions with two distinct states and size-dependent relative populations. The origins of each state were assigned on the basis of photodetachment cross sections and density functional calculations. The two states in the (formamide) $_n^-$  spectra are more than 1 eV apart, with the higher binding energy peak dominating for all but one cluster size ( $n = 9$ ). As with  $(\text{CH}_3\text{CN})_n^-$ , the lower binding energy features are attributed to a solvated electron state, and higher binding energy states to covalently bound anions. Photodetachment from the low binding energy isomer was also seen to be more efficient from the fast fraction of the mass packet, suggesting that this species is formed shortly after electron attachment, while the more tightly bound isomer forms after a nonadiabatic transition. As discussed above, the photoelectron spectra of acetonitrile cluster anions are dominated by the dimer anion for  $n \geq 13$ . However, for formamide cluster anions, the relative populations are much more similar over a larger range.

Both (acetamide) $_n^-$  and (propionamide) $_n^-$  also bind the excess electron in multiple ways, however none of these appears to be a candidate for a solvated electron. Density functional calculations show that peaks in the photoelectron spectra are consistent with the electron binding to the clusters through collective multipolar interactions in either a "straight" or a "folded" arrangement of the hydrogen bond network. This situation is more similar to that of cluster anions of aromatic solvent molecules, such as pyridine and anthracene, discussed in the next section.

## 7. BENZENE, TOLUENE, AND OTHER AROMATIC SOLVENTS

While the majority of solvated electron studies have been conducted in polar or weakly polar solvents, excess electrons can be stabilized by aggregates of nonpolar molecules. Kaya and co-workers<sup>48</sup> have studied the negative ions of benzene ( $\text{C}_6\text{H}_6$ ) and toluene ( $\text{C}_7\text{H}_8$ ) clusters to this end and analyzed their results in the context of an electrostatic model. These (benzene) $_n^-$  and (toluene) $_n^-$  clusters were each investigated using two different ionization techniques: a thermal electron source provided high-energy electron impacts, while photoelectric emission from an irradiated  $\text{Y}_2\text{O}_3$  disk provided very low ( $\sim 0.3$  eV) kinetic energy electrons for direct association with the clusters. For large sizes, there were no significant differences in the TOF cluster distribution, with the clusters resolvable up to  $n = 200$ . The low energy method produced anionic clusters starting at  $n = 53$  for benzene and  $n = 25$  for toluene, in stark contrast to  $(\text{H}_2\text{O})_n^-$  which begins with the water dimer anion. The higher impact energy method, however, generated clusters as small as  $n = 2-10$ . These were assigned to fragmentation of the larger clusters which had been given more internal energy from the capture of faster electrons, for example,  $(\text{benzene})_m^- \rightarrow (\text{benzene})_n^- + (m-n)(\text{benzene})$ . The smaller fragments are likely metastable on the time scale of their experiment, as they could not be produced directly. Representative mass spectra are shown in Figure 20.

Neither benzene nor toluene molecules stably bind an excess electron at the minimum energy neutral geometry, as their vertical electron affinities are both negative.<sup>266,267</sup> However, it is

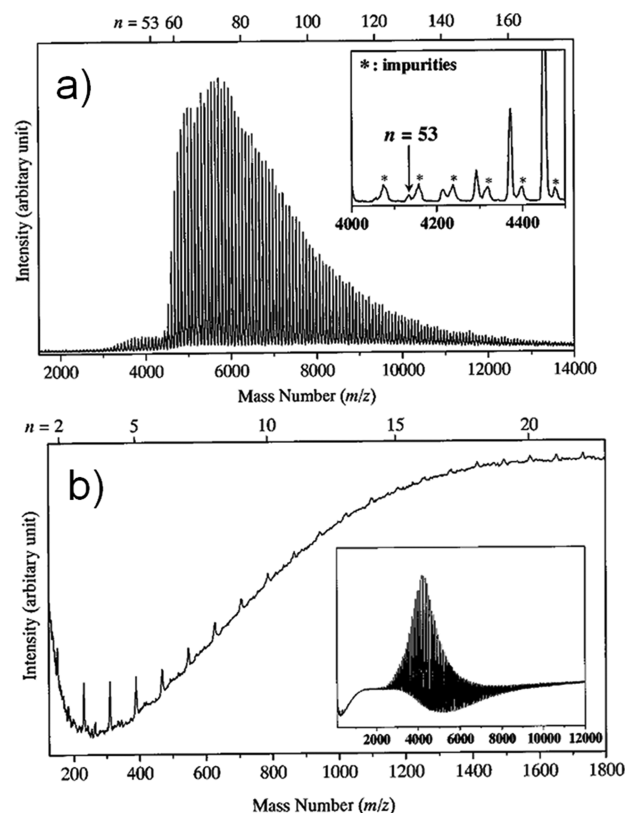


**Figure 20.** Time-of-flight mass spectrum of (benzene) $_n^-$  using (a) tunable low energy electron impact ionization and (b) high-energy electron impact ionization. Smaller clusters are observed in the low impact energy mass spectrum due to fragmentation of the larger, hot clusters. Reprinted with permission from ref 48. Copyright 2002 American Institute of Physics.

unknown if there is a geometry that would produce a positive adiabatic electron affinity. Dissociative electron association studies<sup>268</sup> have shown a resonance around 0.3 eV for benzene, which suggests the smaller clusters could be a distorted benzene anion stabilized by solvation. If this state exists it is likely short-lived as these clusters are not produced by the direct ionization method.

Photoelectron spectroscopy<sup>48</sup> of these cluster anions shows that in both cases the excess electron is only weakly bound to the nonpolar clusters, having a binding energy of only  $0.568 \pm 0.020$  eV for (benzene) $_{124}^-$  and  $0.630 \pm 0.021$  eV for (toluene) $_{139}^-$ , the largest of these clusters measured. Extrapolation of these VDEs yields bulk values of 0.84 and 0.90 eV, respectively (see Figure 4). These values are lower than all other solvated electron clusters considered to bind the electron internally, specifically water and methanol, but are comparable to ammonia. The appearance of the smaller metastable clusters suggests the presence of shallow potential wells in or around the cluster. Because there is no strong permanent dipole for either molecule (toluene has a weak dipole moment of 0.37 D<sup>259</sup>), large, nearly spherical clusters will also have almost no net polarity. Thus polarization and higher-order multipolar effects must come into play in order to bind the excess electron. Other effects, such as a charge-resonance leading to a dimer anion core have also been examined, but the success of the dielectric continuum model suggests a more diffuse state. Only small adjustments to the solvent molecule hard-sphere radius need to be made to give excellent quantitative agreement

between the experiment and DC theory using dielectric values for liquid benzene and toluene. An increase in the radius from 3.0 to 3.2 Å reproduces the correct slope, indicating that the clusters are at a lower density than expected. This is likely a common phenomenon in solvent cluster anions as the solvent structure changes slightly to accommodate the equilibrium charge distribution.<sup>46</sup> As Kaya and co-workers note, the fact that the dielectric continuum models produce relatively good agreement for both of these solvents is interesting considering that the effective radii are sensitive to temperature and density, while the dielectric constants are not.

Photoelectron spectra of cluster anions comprising other aromatic species (naphthalene, anthracene, pyridine, pyrimidine) have been examined to look for possible solvated electron clusters. However, these solvents tend to bind the excess electron to the valence orbitals of one or two molecules which then become solvated themselves, similar to the case of the acetonitrile dimer anion (isomer II). For example, negative ions of pyridine<sup>269</sup> and naphthalene<sup>270</sup> clusters both consist of a solvated monomer anion core, while pyrazine<sup>271</sup> and anthracene<sup>272</sup> can have the charge localized on dimer or trimer anions, and thus are not true solvated electron clusters.

## 8. TETRAHYDROFURAN

Electron solvation in tetrahydrofuran (THF, C<sub>4</sub>H<sub>8</sub>O) has been studied extensively by transient absorption experiments and mixed quantum/classical simulations. THF is “weakly polar” in that it has a small static dielectric constant but has a sizable permanent dipole (1.64–1.75 D in liquid).<sup>259,273</sup> This, combined with its unique liquid structure dramatically affects the way in which electrons are solvated within the ether. The ring structure of THF makes packing inefficient and leads to large pockets of empty space between the solvent molecules, which act as preformed cavities for the electrons to occupy without vastly disrupting the solvent structure. Molecular dynamics simulations<sup>274</sup> predict and neutron scattering experiments<sup>275</sup> show that these voids can be between 2 and 5 Å across (atom-to-atom) and are partially positively polarized.

Experimentally, the excess electron in THF is generated by CTTS excitation from a solvated inorganic ion. Transient absorption experiments by the groups of Schwartz and Ruhman have employed the chemically exotic alkali metal anions M<sup>-</sup> to this effect.<sup>276,277</sup> Schwartz and co-workers<sup>278,279</sup> have also utilized iodide as a source for electrons to investigate the effect of different symmetry of the CTTS state on the relaxation dynamics.

While extensive studies on the nature of the solvated electron excited state and its relaxation have been carried out, less attention has focused on the binding energy of the ground state and the minimum number of solvent molecules needed to support it. To this end, Neumark and co-workers<sup>92</sup> studied the photoelectron spectra of (THF)<sub>n</sub><sup>-</sup> (1 ≤ n ≤ 100). Beyond n ≥ 6 the spectra take on the typical broad, asymmetric line shape of solvated electron clusters. Importantly, no other isomers were observed when the source conditions were modified as was seen for water and methanol cluster anions. The smaller clusters (n = 1–5) in the mass spectrum likely arise from fragmentation of the larger aggregates, similar to what Kaya and co-workers suggested for the presence of small benzene and toluene cluster anions when using a similar anion cluster source.<sup>48</sup>

The VDEs versus n<sup>-1/3</sup> are shown along with the other solvents and measured bulk binding energies in Figure 4.

Extrapolation yields a bulk VDE of 3.10 ± 0.03 eV. This number is consistent with photoelectron spectroscopy of liquid THF jets at room temperature,<sup>280</sup> suggesting that the larger clusters possess a liquid structure. The slopes and intercepts calculated from dielectric continuum theory do not quantitatively reproduce the experimental data, even when corrected for the lower temperature of the anion beam using temperature-dependent parameters. Importantly, the VDE for (THF)<sub>6</sub><sup>-</sup> is 1.96 eV, much higher than for other comparably sized solvent cluster anions. For example, (H<sub>2</sub>O)<sub>15</sub><sup>-</sup> has a VDE of ~0.91 eV,<sup>177</sup> while (benzene)<sub>53</sub><sup>-</sup> is even lower, around 0.47 eV.<sup>48</sup> The slope of VDEs versus n<sup>-1/3</sup> is also fairly small, about -1.74 eV which implies that additional solvent molecules do not have a large effect on stabilizing the excess charge (compare this to ~5.7–6.6 eV for water clusters).

The propensity for neat THF in the bulk to form positively polarized cavities suggests that sufficiently large neutral clusters should do the same thing. These voids can act as pre-existing traps for the electrons to be readily attached, requiring little orientational relaxation. The small slope and large VDE of the first identifiable THF solvated electron cluster are consistent with this idea, since the neutral structure would not be largely perturbed by the electron, and thus not be largely stabilized by additional solvent molecules. Failure of the continuum model is also expected in this situation, since the void structure in the liquid is inherently molecular in nature, owing to the frustrated packing of the rings. The lack of other isomers is also consistent with deep, pre-existing potential energy wells accessible to the electron after attachment.

More insight on the solvent structure and solvation process can be obtained from time-resolved experiments on the excited state and charge-transfer dynamics along with high quality computational studies. Recent photoelectron spectroscopy work in conjunction with MD/ab initio calculations on Γ(THF)<sub>n</sub> clusters<sup>119</sup> shows that beginning around n = 7–9 the iodide becomes only partially embedded within the cluster due to the inefficient packing of the solvent. This incomplete solvent shell persists at least to the n = 20–30 range. CTTS states have also been observed for clusters as small as n = 4, laying the stage for charge transfer studies in the near future. The effect of the solvent packing on the excited state and charge transfer dynamics and the possibility of the excited state wave function penetrating into secondary solvent cavities is of particular interest.<sup>274</sup>

## 9. SUMMARY AND OUTLOOK

We have presented much of the recent work on the dynamics of excess electrons in solvent clusters, along with less comprehensive discussions of their spectroscopy and structure. Anionic solvent cluster binding energies and geometries can be elucidated using a variety of theoretical and spectroscopic techniques, the results of which are fundamental to the understanding of the dynamics of excess electrons in those systems. These studies provide a crucial complement to condensed phase work and give important insight and molecular level detail not available in the liquid phase.

Forthcoming experiments on solvated electrons in clusters will focus on a variety of different avenues. As shown by Beyer and co-workers,<sup>281</sup> the reactivity of the solvated electron can be studied directly in the gas phase using the solvent cluster anion as a size-tunable solvent environment. These experiments suggest that the role of solvated electron in low-energy DNA damage can be elucidated by doping a water cluster with a

DNA base and then injecting an electron by photoinduced charge transfer while monitoring the cluster binding energy. Recently, the observation of water cluster dianions was reported by Cheshnovsky and co-workers,<sup>176</sup> which are proposed as gas-phase analogs to the solvated dielectron system. Calculations show the two electrons to have significantly different binding energies owing to the Coulomb repulsion between the charges. One-photon and time-resolved photoelectron spectroscopy studies on these dianions are of considerable interest.

The advent of photoelectron spectroscopy of liquid micro-jets<sup>8,41</sup> has allowed for the connection between solvent cluster anions and bulk solvated electrons to be directly addressed. Future experiments on the dynamics of internal conversion in water are of significant interest, as well as exploring electron binding in other solvents. Advances in free electron and table-top laser technology will no doubt enable more sensitive probes to the local solvation environment within the cluster, while increases in time-resolution will penetrate deeper into the earliest stages of the relaxation and solvation processes. New and more advanced pseudopotentials will allow for greater detail into the solvation process itself in many clusters to be seen, while increasingly powerful computers will extend the range of tractable sizes.

Solvent cluster anions and the related species considered here are an important paradigm in cluster science, addressing the key issue of how the spectroscopy and dynamics of the solvated electron evolve from finite systems as the bulk limit is approached. Experimental and theoretical investigations of this problem are likely to be a fruitful and rewarding endeavor for quite some time.

## AUTHOR INFORMATION

### Corresponding Author

\*E-mail: dneumark@berkeley.edu.

### Present Address

§Argonne-Northwestern Solar Energy Research (ANSER) Center, Northwestern University, Evanston, IL 60208

### Notes

The authors declare no competing financial interest.

### Biographies



Ryan Young was born in 1983 in Midland, Texas. He studied chemistry and physics at the University of California, Los Angeles as an Arnold & Mabel Beckman Scholar, receiving a B.S. in Chemistry in 2006. He then went on to study anion dynamics using time-resolved photoelectron imaging at the University of California, Berkeley in the

group of Daniel Neumark, receiving his Ph.D. in 2011. Currently, he is the Camille & Henry Dreyfus Postdoctoral Fellow in Environmental Chemistry at the Argonne-Northwestern Solar Energy Research (ANSER) Center at Northwestern University in the group of Dick Co and Michael Wasielewski, where he is studying the structural dynamics mediating charge transfer using femtosecond stimulated Raman spectroscopy.



Daniel Neumark was born in 1955 in Chicago, IL. He was an undergraduate of Harvard University, where he earned a B.A. in Chemistry and Physics and an M.A. in Chemistry in 1977. During his time at Harvard he carried out undergraduate research with Prof. Dudley Herschbach. He spent a year in Cambridge University working with Prof. A.D. Buckingham. He was a graduate student at the University of California, Berkeley in the research group of Prof. Yuan Lee, and received his Ph.D. in 1984. He then carried out post-doctoral research at the University of Colorado, Boulder, with Prof. W. Carl Lineberger. In 1986, he joined the faculty of the Chemistry Department at U.C. Berkeley, and has been there ever since. Professor Neumark's research interests focus on the spectroscopy and dynamics of negative ions, clusters, and liquid jets. He is best known for experiments in which he used negative ion photodetachment to probe and characterize the transition state of chemical reactions, and for the development of time-resolved photoelectron spectroscopy of negative ions. He is a Fellow of the American Physical Society, the American Association for the Advancement of Science, and the American Academy of Arts and Sciences. He has received the ACS Nobel Laureate Signature Award (with Martin Zanni), the Bomem-Michelson Award, the William F. Meggers Award, the Irving Langmuir Award in Chemical Physics, and the Herschbach Medal. He was Director of the Chemical Sciences Division at Lawrence Berkeley National Laboratory from 2000–2010, and is currently Chair of the Chemistry Department at Berkeley.

## ACKNOWLEDGMENTS

This work is supported by the National Science Foundation under Grant No. CHE-1011819. DMN thanks the many graduate students and postdoctoral fellows who carried out the work in his laboratory that is reported here, and thanks Ori Cheshnovsky and Rainer Weinkauff for very fruitful collaborations in this area of research.

## REFERENCES

- (1) Gordon, S.; Thomas, J. K.; Matheson, M. S.; Rabani, J.; Hart, E. J. *J. Am. Chem. Soc.* **1963**, *85*, 1375.
- (2) Arnold, F. *Nature* **1981**, *294*, 732.
- (3) Birch, A. J. *J. Chem. Soc.* **1944**, 430.
- (4) Berdys, J.; Anusiewicz, I.; Skurski, P.; Simons, J. *J. Am. Chem. Soc.* **2004**, *126*, 6441.

- (5) Thomas, S. J. M.; Edwards, P. P.; Kuznetsov, V. L. *ChemPhysChem* **2008**, *9*, 59.
- (6) Weyl, W. *Ann. Phys.* **1864**, *199*, 350.
- (7) Hart, E. J.; Anbar, M. *The Hydrated Electron*; Wiley-Interscience: New York, 1970.
- (8) Abel, B.; Buck, U.; Sobolewski, A. L.; Domcke, W. *Phys. Chem. Chem. Phys.* **2012**, *14*, 22.
- (9) Kevan, L. *Chem. Phys. Lett.* **1979**, *66*, 578.
- (10) Kevan, L. *Acc. Chem. Res.* **1981**, *14*, 138.
- (11) Hameka, H. F.; Robinson, G. W.; Marsden, C. J. *J. Phys. Chem.* **1987**, *91*, 3150.
- (12) Sobolewski, A. L.; Domcke, W. *Phys. Chem. Chem. Phys.* **2007**, *9*, 3818.
- (13) Larsen, R. E.; Glover, W. J.; Schwartz, B. J. *Science* **2010**, *329*, 65.
- (14) Turi, L.; Madarász, A. *Science* **2011**, *331*, 1387.
- (15) Larsen, R. E.; Glover, W. J.; Schwartz, B. J. *Science* **2011**, *331*, 1387.
- (16) Jacobson, L. D.; Herbert, J. M. *Science* **2011**, *331*, 1387.
- (17) Lindner, J.; Unterreiner, A.-N.; Vöhringer, P. *ChemPhysChem* **2006**, *7*, 363.
- (18) Kevan, L. *J. Phys. Chem.* **1972**, *76*, 3830.
- (19) Arai, S.; Myran, C. Sauer, J. *J. Chem. Phys.* **1966**, *44*, 2297.
- (20) Kummrov, A.; Emde, M. F.; Baltuska, A.; Pshenichnikov, M. S.; Wiersma, D. A. *J. Phys. Chem. A* **1998**, *102*, 4171.
- (21) Pshenichnikov, M. S.; Baltuska, A.; Wiersma, D. A. *Chem. Phys. Lett.* **2004**, *389*, 171.
- (22) Pshenichnikov, M. S.; Baltuska, A.; Wiersma, D. A. *Top. Appl. Phys.* **2004**, *95*, 409.
- (23) Alfano, J. C.; Walhout, P. K.; Kimura, Y.; Barbara, P. F. *J. Chem. Phys.* **1993**, *98*, 5996.
- (24) Kimura, Y.; Alfano, J. C.; Walhout, P. K.; Barbara, P. F. *J. Phys. Chem.* **1994**, *98*, 3450.
- (25) Schwartz, B. J.; Rossky, P. J. *J. Chem. Phys.* **1994**, *101*, 6917.
- (26) Walhout, P. K.; Alfano, J. C.; Kimura, Y.; Silva, C.; Reid, P. J.; Barbara, P. F. *Chem. Phys. Lett.* **1995**, *232*, 135.
- (27) Silva, C.; Walhout, P. K.; Yokoyama, K.; Barbara, P. *Phys. Rev. Lett.* **1998**, *80*, 1086.
- (28) Yokoyama, K.; Silva, C.; Son, D. H.; Walhout, P. K.; Barbara, P. *J. Phys. Chem. A* **1998**, *102*, 6957.
- (29) Castleman, A. W., Jr.; Bowen, K. H., Jr. *J. Phys. Chem.* **1996**, *100*, 12911.
- (30) Jortner, J. *Faraday Discuss.* **1997**, *1*.
- (31) Castleman, A. W.; Mark, T. D. *Adv. At. Mol. Phys.* **1985**, *20*, 65.
- (32) Neumark, D. M. *Mol. Phys.* **2008**, *106*, 2183.
- (33) Ehrler, O. T.; Neumark, D. M. *Acc. Chem. Res.* **2009**, *42*, 769.
- (34) Makov, G.; Nitzan, A. *J. Phys. Chem.* **1994**, *98*, 3459.
- (35) Zharikov, A. A.; Fischer, S. F. *J. Chem. Phys.* **2007**, *126*, 134707.
- (36) Klots, C. E. *J. Phys. Chem.* **1988**, *92*, 5864.
- (37) Klots, C. E. *Chem. Phys. Lett.* **1991**, *186*, 73.
- (38) Asmis, K. R.; Brummer, M.; Kaposta, C.; Santambrogio, G.; von Helden, G.; Meijer, G.; Rademann, K.; Woste, L. *Phys. Chem. Chem. Phys.* **2002**, *4*, 1101.
- (39) Wang, X. B.; Wang, L. S. *Rev. Sci. Instrum.* **2008**, *79*, 073108.
- (40) Ma, L.; Majer, K.; Chirof, F.; Issendorff, B. v. *J. Chem. Phys.* **2009**, *131*, 144303.
- (41) Winter, B.; Faubel, M. *Chem. Rev.* **2006**, *106*, 1176.
- (42) Siefertmann, K. R.; Liu, Y.; Lugovoy, E.; Link, O.; Faubel, M.; Buck, U.; Winter, B.; Abel, B. *Nat. Chem.* **2010**, *2*, 274.
- (43) Bragg, A. E.; Verlet, J. R. R.; Kammrath, A.; Cheshnovsky, O.; Neumark, D. M. *Science* **2004**, *306*, 669.
- (44) Johnson, M. A.; Alexander, M. L.; Lineberger, W. C. *Chem. Phys. Lett.* **1984**, *112*, 285.
- (45) Tsukuda, T.; Saeki, M.; Iwata, S.; Nagata, T. *J. Phys. Chem. A* **1997**, *101*, 5103.
- (46) Sarkas, H. W.; Arnold, S. T.; Eaton, J. G.; Lee, G. H.; Bowen, K. H. *J. Chem. Phys.* **2002**, *116*, 5731.
- (47) Garand, E.; Yacovitch, T. I.; Neumark, D. M. *J. Chem. Phys.* **2009**, *130*, 064304.
- (48) Mitsui, M.; Nakajima, A.; Kaya, K. *J. Chem. Phys.* **2002**, *117*, 9740.
- (49) Mitsuke, K.; Kondow, T.; Kuchitsu, a. K. *J. Phys. Chem.* **1986**, *90*, 1505.
- (50) Kondow, T. *J. Phys. Chem.* **1987**, *91*, 1307.
- (51) Coe, J. V.; Lee, G. H.; Eaton, J. G.; Arnold, S. T.; Sarkas, H. W.; Bowen, K. H.; Ludewigt, C.; Haberland, H.; Worsnop, D. R. *J. Chem. Phys.* **1990**, *92*, 3980.
- (52) Johnson, M. A.; Lineberger, W. C. In *Techniques of Chemistry*; Farrar, J. M., Saunders, W. H., Jr., Eds.; Wiley: New York, 1988; Vol. 20.
- (53) Proch, R.; Trickl, T. *Rev. Sci. Instrum.* **1989**, *60*, 713.
- (54) Even, U.; Jortner, J.; Noy, D.; Lavie, N.; Cossart-Magos, C. *J. Chem. Phys.* **2000**, *112*, 8068.
- (55) D. Hern Paik, I.-R. L.; Yang, D.-S.; Baskin, J. S.; Zewail, A. H. *Science* **2004**, *306*, 672.
- (56) Leopold, D. G.; Ho, J.; Lineberger, W. C. *J. Chem. Phys.* **1987**, *86*, 1715.
- (57) Wiley, W. C.; McLaren, I. H. *Rev. Sci. Instrum.* **1955**, *26*, 1150.
- (58) Karataev, V. I.; Shmikk, D. V.; Mamyrin, B. A. *Sov. Phys. Tech. Phys. USSR* **1972**, *16*, 1177.
- (59) Boesl, U.; Weinkauff, R.; Schlag, E. W. *Int. J. Mass Spectrom. Ion Process.* **1992**, *112*, 121.
- (60) Engelking, P. C.; Ellison, G. B.; Lineberger, W. C. *J. Chem. Phys.* **1978**, *69*, 1826.
- (61) Ichino, T.; Wren, S. W.; Vogelhuber, K. M.; Gianola, A. J.; Lineberger, W. C.; Stanton, J. F. *J. Chem. Phys.* **2008**, *129*.
- (62) Dillon, J.; Yarkony, D. R.; Schuurman, M. S. *J. Chem. Phys.* **2011**, *134*.
- (63) Cooper, J.; Zare, R. N. *J. Chem. Phys.* **1968**, *48*, 942.
- (64) Reid, K. L. *Annu. Rev. Phys. Chem.* **2003**, *54*, 397.
- (65) Siegel, M. W.; Celotta, R. J.; Hall, J. L.; Levine, J.; Bennett, R. A. *Phys. Rev. A* **1972**, *6*, 607.
- (66) Leopold, D. G.; Murray, K. K.; Miller, A. E. S.; Lineberger, W. C. *J. Chem. Phys.* **1985**, *83*, 4849.
- (67) Ervin, K. M.; Lineberger, W. C. *J. Phys. Chem.* **1991**, *95*, 1167.
- (68) Posey, L. A.; Deluca, M. J.; Johnson, M. A. *Chem. Phys. Lett.* **1986**, *131*, 170.
- (69) Metz, R. B.; Weaver, A.; Bradforth, S. E.; Kitsopoulos, T. N.; Neumark, D. M. *J. Phys. Chem.* **1990**, *94*, 1377.
- (70) Xu, C.; Burton, G. R.; Taylor, T. R.; Neumark, D. M. *J. Chem. Phys.* **1998**, *108*, 7645.
- (71) Kim, J.; Becker, I.; Cheshnovsky, O.; Johnson, M. A. *Chem. Phys. Lett.* **1998**, *297*, 90.
- (72) Kruit, P.; Read, F. H. *J. Phys. E* **1983**, *16*, 313.
- (73) Cheshnovsky, O.; Yang, S. H.; Pettiette, C. L.; Craycraft, M. J.; Smalley, R. E. *Rev. Sci. Instrum.* **1987**, *58*, 2131.
- (74) Wang, L. S.; Ding, C. F.; Wang, X. B.; Barlow, S. E. *Rev. Sci. Instrum.* **1999**, *70*, 1957.
- (75) Hotop, H.; Lineberger, W. C. *J. Phys. Chem. Ref. Data* **1985**, *14*, 731.
- (76) Mitsui, M.; Ando, N.; Kokubo, S.; Nakajima, A.; Kaya, K. *Phys. Rev. Lett.* **2003**, *91*, 153002.
- (77) Maeyama, T.; Negishi, Y.; Tsukuda, T.; Yagi, I.; Mikami, N. *Phys. Chem. Chem. Phys.* **2006**, *8*, 827.
- (78) Maeyama, T.; Yoshida, K.; Fujii, A. *J. Phys. Chem. A* **2012**, *116*, 3771.
- (79) Baguenard, B.; Pinare, J. C.; Bordas, C.; Broyer, M. *Phys. Rev. A* **2001**, *6302*, 3204.
- (80) Baguenard, B.; Pinare, J. C.; Lepine, F.; Bordas, C.; Broyer, M. *Chem. Phys. Lett.* **2002**, *352*, 147.
- (81) Surber, E.; Sanov, A. *J. Chem. Phys.* **2002**, *116*, 5921.
- (82) Surber, E.; Sanov, A. *Phys. Rev. Lett.* **2003**, *90*, 3001.
- (83) Chandler, D. W.; Houston, P. L. *J. Chem. Phys.* **1987**, *87*, 1445.
- (84) Heck, A. J. R.; Chandler, D. W. *Annu. Rev. Phys. Chem.* **1995**, *46*, 335.
- (85) Helm, H.; Bjerre, N.; Dyer, M. J.; Huestis, D. L.; Saeed, M. *Phys. Rev. Lett.* **1993**, *70*, 3221.

- (86) Eppink, A. T. J. B.; Parker, D. H. *Rev. Sci. Instrum.* **1997**, *68*, 3477.
- (87) Dribinski, V.; Ossadtchi, A.; Mandelshtam, V. A.; Reisler, H. *Rev. Sci. Instrum.* **2002**, *73*, 2634.
- (88) Garcia, G. A.; Nahon, L.; Powis, I. *Rev. Sci. Instrum.* **2004**, *75*, 4989.
- (89) Verlet, J. R. R.; Bragg, A. E.; Kammrath, A.; Cheshnovsky, O.; Neumark, D. M. *Science* **2005**, *307*, 93.
- (90) Kammrath, A.; Verlet, J. R. R.; Griffin, G. B.; Neumark, D. M. *J. Chem. Phys.* **2006**, *125*, 171102.
- (91) Young, R. M.; Griffin, G. B.; Kammrath, A.; Ehrler, O. T.; Neumark, D. M. *Chem. Phys. Lett.* **2010**, *485*, 59.
- (92) Young, R. M.; Yandell, M. A.; Niemeyer, M.; Neumark, D. M. *J. Chem. Phys.* **2010**, *133*, 154312.
- (93) Asmis, K. R.; Santambrogio, G.; Zhou, J.; Garand, E.; Headrick, J.; Goebbert, D.; Johnson, M. A.; Neumark, D. M. *J. Chem. Phys.* **2007**, *126*, 191105.
- (94) Robertson, W. H.; Johnson, M. A. *Annu. Rev. Phys. Chem.* **2003**, *54*, 173.
- (95) Duncan, M. A. *Int. J. Mass. Spectrom.* **2000**, *200*, 545.
- (96) Headrick, J. M.; Diken, E. G.; Walters, R. S.; Hammer, N. I.; Christie, R. A.; Cui, J.; Myshakin, E. M.; Duncan, M. A.; Johnson, M. A.; Jordan, K. D. *Science* **2005**, *308*, 1765.
- (97) Guasco, T. L.; Elliott, B. M.; Johnson, M. A.; Ding, J.; Jordan, K. D. *J. Phys. Chem. Lett.* **2010**, *1*, 2396.
- (98) Oepts, D.; van der Meer, A. F. G.; van Amersfoort, P. W. *Infrared Phys. Technol.* **1995**, *36*, 297.
- (99) Bush, M. F.; O'Brien, J. T.; Prell, J. S.; Saykally, R. J.; Williams, E. R. *J. Am. Chem. Soc.* **2007**, *129*, 1612.
- (100) O'Brien, J. T.; Prell, J. S.; Bush, M. F.; Williams, E. R. *J. Am. Chem. Soc.* **2010**, *132*, 8248.
- (101) Price, W. D.; Schnier, P. D.; Williams, E. R. *Anal. Chem.* **1996**, *68*, 859.
- (102) Suzuki, T.; Whitaker, B. J. *Int. Rev. Phys. Chem.* **2001**, *20*, 313.
- (103) Stolow, A. *Int. Rev. Phys. Chem.* **2003**, *22*, 377.
- (104) Stolow, A.; Bragg, A. E.; Neumark, D. M. *Chem. Rev.* **2004**, *104*, 1719.
- (105) Barnett, R. N.; Landman, U.; Cleveland, C. L.; Jortner, J. *Chem. Phys. Lett.* **1988**, *145*, 382.
- (106) Stampfli, P.; Bennemann, K. H. *Phys. Rev. Lett.* **1987**, *58*, 2635.
- (107) Coe, J. V.; Lee, G. H.; Eaton, J. G.; Arnold, S. T.; Sarkas, H. W.; Bowen, K. H.; Ludewigt, C.; Haberland, H.; Worsnop, D. R. *J. Chem. Phys.* **1990**, *92*, 3980.
- (108) Barnett, R. N.; Landman, U.; Cleveland, C. L.; Jortner, J. *J. Chem. Phys.* **1988**, *88*, 4429.
- (109) Jordan, K. D.; Wang, F. *Annu. Rev. Phys. Chem.* **2003**, *54*, 367.
- (110) Marsalek, O.; Uhlig, F.; VandeVondele, J.; Jungwirth, P. *Acc. Chem. Res.* **2012**, *45*, 23.
- (111) Herbert, J. M.; Jacobson, L. D. *Int. Rev. Phys. Chem.* **2011**, *30*, 1.
- (112) Lee, S.; Kim, J.; Lee, S. J.; Kim, K. S. *Phys. Rev. Lett.* **1997**, *79*, 2038.
- (113) Herbert, J. M.; Head-Gordon, M. *Proc. Natl. Acad. Sci.* **2006**, *103*, 14282.
- (114) Sommerfeld, T.; Gardner, S. D.; DeFusco, A.; Jordan, K. D. *J. Chem. Phys.* **2006**, *125*, 174301.
- (115) Roscioli, J. R.; Hammer, N. I.; Johnson, M. A.; Diri, K.; Jordan, K. D. *J. Chem. Phys.* **2008**, *128*, 104314.
- (116) Kim, J.; Park, J. M.; Oh, K. S.; Lee, J. Y.; Lee, S.; Kim, K. S. *J. Chem. Phys.* **1997**, *106*, 10207.
- (117) Herbert, J. M.; Head-Gordon, M. *J. Phys. Chem. A* **2005**, *109*, 5217.
- (118) Frigato, T.; VandeVondele, J.; Schmidt, B.; Schutte, C.; Jungwirth, P. *J. Phys. Chem. A* **2008**, *112*, 6125.
- (119) Young, R. M.; Azar, R. J.; Yandell, M. A.; King, S. B.; Head-Gordon, M.; Neumark, D. M. *Mol. Phys.* **2012**, *1*.
- (120) Barnett, R. N.; Landman, U.; Cleveland, C. L.; Jortner, J. *J. Chem. Phys.* **1988**, *88*, 4421.
- (121) Turi, L.; Borgis, D. *J. Chem. Phys.* **2002**, *117*, 6186.
- (122) Jortner, J.; Ottolenghi, M.; Stein, G. *J. Phys. Chem.* **1964**, *68*, 247.
- (123) Turi, L.; Sheu, W.-S.; Rossky, P. J. *Science* **2005**, *309*, 914.
- (124) Mones, L.; Rossky, P. J.; Turi, L. *J. Chem. Phys.* **2010**, *133*, 144510.
- (125) Schnitker, J.; Rossky, P. J. *J. Chem. Phys.* **1987**, *86*, 3471.
- (126) Herbert, J. M.; Jacobson, L. D. *J. Phys. Chem. A* **2011**, *115*, 14470.
- (127) Sprik, M.; Impey, R. W.; Klein, M. L. *J. Chem. Phys.* **1985**, *83*, 5802.
- (128) Marchi, M.; Sprik, M.; Klein, M. L. *J. Chem. Phys.* **1988**, *89*, 4918.
- (129) Marsalek, O.; Uhlig, F.; Frigato, T.; Schmidt, B.; Jungwirth, P. *Phys. Rev. Lett.* **2010**, *105*, 043002.
- (130) Madarász, Á.; Rossky, P. J.; Turi, L. *J. Chem. Phys.* **2009**, *130*, 124319.
- (131) Mones, L.; Rossky, P. J.; Turi, L. *J. Chem. Phys.* **2011**, *135*, 084501.
- (132) Jacobson, L. D.; Herbert, J. M. *J. Am. Chem. Soc.* **2011**, *133*, 19889.
- (133) Bartels, D. M. *J. Chem. Phys.* **2001**, *115*, 4404.
- (134) Jacobson, L. D.; Herbert, J. M. *J. Chem. Phys.* **2010**, *133*, 154506.
- (135) Kevan, L. *Acc. Chem. Res.* **1980**, *14*, 138.
- (136) Hart, E. J.; Boag, J. W. *J. Am. Chem. Soc.* **1962**, *84*, 4090.
- (137) Boero, M.; Parrinello, M.; Terakura, K.; Ikeshoji, T.; Liew, C. C. *Phys. Rev. Lett.* **2003**, *90*, 226403.
- (138) Migus, A.; Gauduel, Y.; Martin, J. L.; Antonetti, A. *Phys. Rev. Lett.* **1987**, *58*, 1559.
- (139) Shi, X.; Long, F. H.; Lu, H.; Eienthal, K. B. *J. Phys. Chem.* **1996**, *100*, 11903.
- (140) Hertwig, A.; Hippler, H.; Unterreiner, A. N.; Vohringer, P. *Ber. Bunsen-Ges. Phys. Chem.* **1998**, *102*, 805.
- (141) Assel, M.; Laenen, R.; Laubereau, A. *J. Phys. Chem. A* **1998**, *102*, 2256.
- (142) Thaller, A.; Laenen, R.; Laubereau, A. *Chem. Phys. Lett.* **2004**, *398*, 459.
- (143) Schwartz, B. J.; Rossky, P. J. *J. Chem. Phys.* **1994**, *101*, 6902.
- (144) Long, F. H.; Shi, X. L.; Lu, H.; Eienthal, K. B. *J. Phys. Chem.* **1994**, *98*, 7252.
- (145) Gauduel, Y.; Gelabert, H.; Ashokkumar, M. *Chem. Phys.* **1995**, *197*, 167.
- (146) Chen, X.; Bradforth, S. E. *Annu. Rev. Phys. Chem.* **2007**, *59*, 203.
- (147) Blandamer, M. J.; Fox, M. F. *Chem. Rev.* **1970**, *70*, 59.
- (148) Haberland, H.; Langosch, H.; Schindler, H. G.; Worsnop, D. R. *J. Phys. Chem.* **1984**, *88*, 3903.
- (149) Posey, L. A.; Johnson, M. A. *J. Chem. Phys.* **1988**, *89*, 4807.
- (150) Desfrancois, C.; Khelifa, N.; Lisfi, A.; Schermann, J. P.; Eaton, J. G.; Bowen, K. H. *J. Chem. Phys.* **1991**, *95*, 7760.
- (151) Desfrancois, C.; Lisfi, A.; Schermann, J. P. *Z. Phys. D* **1992**, *24*, 297.
- (152) Zappa, F.; Denifl, S.; Mähr, I.; Bacher, A.; Echt, O.; Märk, T. D.; Scheier, P. *J. Am. Chem. Soc.* **2008**, *130*, 5573.
- (153) Verlet, J. R. R.; Kammrath, A.; Griffin, G. B.; Neumark, D. M. *J. Chem. Phys.* **2005**, *123*, 4.
- (154) Kammrath, A.; Verlet, J. R. R.; Griffin, G. B.; Neumark, D. M. *J. Chem. Phys.* **2006**, *125*, 076101.
- (155) Coe, J. V.; Arnold, S. T.; Eaton, J. G.; Lee, G. H.; Bowen, K. H. *J. Chem. Phys.* **2006**, *125*, 014315.
- (156) Coe, J. V. *Int. Rev. Phys. Chem.* **2001**, *20*, 33.
- (157) Young, R. M.; Yandell, M. A.; King, S. B.; Neumark, D. M. *J. Chem. Phys.* **2012**, *136*, 094304.
- (158) Hippler, H.; Troe, J.; Wendelken, H. J. *J. Chem. Phys.* **1983**, *78*, 6709.
- (159) Hippler, H.; Lindemann, L.; Troe, J. *J. Chem. Phys.* **1985**, *83*, 3906.
- (160) Misaizu, F.; Tsukamoto, K.; Sanekata, M.; Fuke, K. *Chem. Phys. Lett.* **1992**, *188*, 241.

- (161) Hertel, I. V.; Hüglin, C.; Nitsch, C.; Schulz, C. P. *Phys. Rev. Lett.* **1991**, *67*, 1767.
- (162) Buck, U.; Dauster, I.; Gao, B.; Liu, Z.-f. *J. Phys. Chem. A* **2007**, *111*, 12355.
- (163) Forck, R. M.; Dauster, I.; Schieweck, Y.; Zeuch, T.; Buck, U.; OnCak, M.; SlaviCek, P. *J. Chem. Phys.* **2010**, *132*, 221102.
- (164) Forck, R. M.; Dauster, I.; Buck, U.; Zeuch, T. *J. Phys. Chem. A* **2011**, *115*, 6068.
- (165) Donald, W. A.; Leib, R. D.; O'Brien, J. T.; Holm, A. I. S.; Williams, E. R. *Proc. Natl. Acad. Sci.* **2008**, *105*, 18102.
- (166) Donald, W. A.; Demireva, M.; Leib, R. D.; Aiken, M. J.; Williams, E. R. *J. Am. Chem. Soc.* **2010**, *132*, 4633.
- (167) Hammer, N. I.; Roscioli, J. R.; Bopp, J. C.; Headrick, J. M.; Johnson, M. A. *J. Chem. Phys.* **2005**, *123*, 244311.
- (168) Hammer, N. I.; Shin, J.-W.; Headrick, J. M.; Diken, E. G.; Roscioli, J. R.; Weddle, G. H.; Johnson, M. A. *Science* **2004**, *306*, 675.
- (169) Roscioli, J. R.; Hammer, N. I.; Johnson, M. A. *J. Phys. Chem. A* **2006**, *110*, 7517.
- (170) Roscioli, J. R.; Hammer, N. I.; Johnson, M. A. *J. Phys. Chem. A* **2006**, *110*, 7517.
- (171) Ayotte, P.; Johnson, M. A. *J. Chem. Phys.* **1997**, *106*, 811.
- (172) Barnett, R. N.; Landman, U.; Cleveland, C. L.; Kestner, N. R.; Jortner, J. *J. Chem. Phys.* **1988**, *88*, 6670.
- (173) Khan, A. *J. Chem. Phys.* **2004**, *121*, 280.
- (174) Lee, H. M.; Suh, S. B.; Tarakeswar, P.; Kim, K. S. *J. Chem. Phys.* **2005**, *122*, 044309.
- (175) Sommerfeld, T.; Jordan, K. D. *J. Am. Chem. Soc.* **2006**, *128*, 5828.
- (176) Barnett, R. N.; Giniger, R.; Cheshnovsky, O.; Landman, U. *J. Phys. Chem. A* **2011**, 7378.
- (177) Bragg, A. E.; Verlet, J. R. R.; Kammrath, A.; Cheshnovsky, O.; Neumark, D. M. *J. Am. Chem. Soc.* **2005**, *127*, 15283.
- (178) Sanov, A.; Mabbs, R. *Int. Rev. Phys. Chem.* **2008**, *27*, 53.
- (179) Marsalek, O.; Uhlig, F.; Jungwirth, P. *J. Phys. Chem. C* **2010**, *114*, 20489.
- (180) Tang, Y.; Shen, H.; Sekiguchi, K.; Kurahashi, N.; Mizuno, T.; Suzuki, Y.-I.; Suzuki, T. *Phys. Chem. Chem. Phys.* **2010**, *12*, 3653.
- (181) Shreve, A. T.; Yen, T. A.; Neumark, D. M. *Chem. Phys. Lett.* **2010**, *493*, 216.
- (182) Lubcke, A.; Buchner, F.; Heine, N.; Hertel, I. V.; Schultz, T. *Phys. Chem. Chem. Phys.* **2010**, *12*, 14629.
- (183) Weber, J. M.; Kim, J.; Woronoowicz, E. A.; Weddle, G. H.; Becker, I.; O, C.; Johnson, M. A. *Chem. Phys. Lett.* **2001**, *339*, 337.
- (184) Fischer, S. F.; Dietz, W. Z. *Phys. Chem* **2007**, *221*, 585.
- (185) Griffin, G. B.; Young, R. M.; Ehrlert, O. T.; Neumark, D. M. *J. Chem. Phys.* **2009**, *131*, 194302.
- (186) Liu, H. T.; Muller, J. P.; Zhavoronkov, N.; Schulz, C. P.; Hertel, I. V. *J. Phys. Chem. A* **2010**, *114*, 1508.
- (187) Zharikov, A. A.; Fischer, S. F. *J. Chem. Phys.* **2006**, *124*, 054506.
- (188) Englman, R.; Jortner, J. *Mol. Phys.* **1970**, *18*, 145.
- (189) Neria, E.; Nitzan, A. *J. Chem. Phys.* **1993**, *99*, 1109.
- (190) Schwartz, B. J.; Rossky, P. J. *J. Chem. Phys.* **1996**, *105*, 6997.
- (191) Serxner, D.; Dessent, C. E. H.; Johnson, M. A. *J. Chem. Phys.* **1996**, *105*, 7231.
- (192) Timerghazin, Q. K.; Peslherbe, G. H. *J. Am. Chem. Soc.* **2003**, *125*, 9904.
- (193) Mak, C. C.; Timerghazin, Q. K.; Peslherbe, G. H. *Phys. Chem. Chem. Phys.* **2012**, *14*, 6257.
- (194) Zanni, M. T.; Lehr, L.; Greenblatt, B. J.; Weinkauff, R.; Neumark, D. M. In *Ultrafast Phenomena XI*; Elsaesser, T., Fujimoto, J. G., Wiersma, D., Zinth, W., Eds.; Springer-Verlag: Berlin, 1998.
- (195) Lehr, L.; Zanni, M. T.; Frischkorn, C.; Weinkauff, R.; Neumark, D. M. *Science* **1999**, *284*, 635.
- (196) Kammrath, A.; Verlet, J. R. R.; Bragg, A. E.; Griffin, G. B.; Neumark, D. M. *J. Phys. Chem. A* **2005**, *109*, 11475.
- (197) Yandell, M. A.; Young, R. M.; King, S. B.; Neumark, D. M. *J. Phys. Chem. A* **2011**, *116*, 2750.
- (198) Takayanagi, T.; Takahashi, K. *Chem. Phys. Lett.* **2006**, *431*, 28.
- (199) Takahashi, K.; Takayanagi, T. *Chem. Phys.* **2007**, *342*, 95.
- (200) Kolaski, M.; Lee, H. M.; Pak, C.; Kim, K. S. *J. Am. Chem. Soc.* **2008**, *130*, 103.
- (201) Lee, H. M.; Suh, S. B.; Kim, K. S. *J. Chem. Phys.* **2003**, *118*, 9981.
- (202) Chen, H.-Y.; Sheu, W.-S. *Chem. Phys. Lett.* **2001**, *335*, 475.
- (203) Vila, F. D.; Jordan, K. D. *J. Phys. Chem.* **2002**, *106*, 1391.
- (204) Provencal, R. A.; Paul, J. B.; Roth, K.; Chapo, C.; Casaes, R. N.; Saykally, R. J. *J. Chem. Phys.* **1999**, *110*, 4258.
- (205) Buck, U.; Huisken, F. *Chem. Rev.* **2000**, *100*, 3863.
- (206) Pepin, C.; Goulet, T.; Houde, D.; Jay-Grin, J.-P. *J. Phys. Chem.* **1994**, *98*, 7009.
- (207) Shi, X.; Long, F. H.; Lu, H.; Eisenthal, K. B. *J. Phys. Chem.* **1995**, *99*, 6917.
- (208) Silva, C.; Wallhout, P. K.; Reid, P. J.; Barbara, P. F. *J. Phys. Chem. A* **1998**, *102*, 5701.
- (209) Vilchiz, V. H.; Chen, X.; Kloepfer, J. A.; Bradforth, S. E. *Radiat. Phys. Chem.* **2005**, *72*, 159.
- (210) Thaller, A.; Laenen, R.; Laubereau, A. *J. Chem. Phys.* **2006**, *124*.
- (211) Tauber, M. J.; Stuart, C. M.; Mathies, R. A. *J. Am. Chem. Soc.* **2004**, *126*, 3414.
- (212) Stuart, C. M.; Tauber, M. J.; Mathies, R. A. *J. Phys. Chem. A* **2007**, *111*, 8390.
- (213) Herrmann, V.; Krebs, P. *J. Phys. Chem.* **1995**, *99*, 6794.
- (214) Shen, H.; Kurahashi, N.; Horio, T.; Sekiguchi, K.; Suzuki, T. *Chem. Lett.* **2010**, *39*, 668.
- (215) Horio, T.; Shen, H.; Adachi, S.; Suzuki, T. *Chem. Phys. Lett.* **2012**, *535*, 12.
- (216) Dauster, I.; Suhm, M. A.; Buck, U.; Zeuch, T. *Phys. Chem. Chem. Phys.* **2008**, *10*, 83.
- (217) Buck, U.; Ettischer, I. *J. Chem. Phys.* **1998**, *108*, 33.
- (218) Natkaniec, I.; Holderna-Natkaniec, K.; Majerz, I.; Parlinski, K. *Chem. Phys.* **2005**, *317*, 171.
- (219) Boyd, S. L.; Boyd, R. J. *J. Chem. Theory Comput.* **2007**, *3*, 54.
- (220) Turi, L. *J. Chem. Phys.* **1999**, *110*, 10364.
- (221) Kammrath, A.; Verlet, J. R. R.; Griffin, G. B.; Neumark, D. M. *J. Chem. Phys.* **2006**, *125*, 171102.
- (222) Mones, L.; Turi, L. *J. Chem. Phys.* **2010**, *132*, 154507.
- (223) Jou, F.-Y.; Freeman, G. R. *J. Phys. Chem.* **1977**, *81*, 909.
- (224) Kammrath, A.; Griffin, G. B.; Verlet, J. R. R.; Young, R. M.; Neumark, D. M. *J. Chem. Phys.* **2007**, *126*, 244306.
- (225) Borgis, D.; Rossky, P. J.; Turi, L. *J. Chem. Phys.* **2006**, *125*, 064501.
- (226) Robertson, W. H.; Karapetian, K.; Ayotte, P.; Jordan, K. D.; Johnson, M. A. *J. Chem. Phys.* **2002**, *116*, 4853.
- (227) Cabarcos, O. M.; Weinheimer, C. J.; Martinez, T. J.; Lisy, J. M. *J. Chem. Phys.* **1999**, *110*, 9516.
- (228) Ayala, R.; Martinez, J. M.; Pappalardo, R. R.; Marcos, E. S. *J. Phys. Chem. A* **2000**, *104*, 2799.
- (229) Beck, J. P.; Lisy, J. M. *J. Phys. Chem. A* **2010**, *114*, 10011.
- (230) Davis, A. V.; Zanni, M. T.; Frischkorn, C.; Neumark, D. M. *J. Electron Spectrosc. Relat. Phenom.* **2000**, *108*, 203.
- (231) Young, R. M.; Yandell, M. A.; Neumark, D. M. *J. Chem. Phys.* **2011**, *134*, 124311.
- (232) Frischkorn, C.; Zanni, M. T.; Davis, A. V.; Neumark, D. M. *Faraday Discuss.* **2000**, *115*, 49.
- (233) Teal, G. K. *Phys. Rev.* **1947**, *71*, 138.
- (234) Bard, A. J.; Itaya, K.; Malpas, R. E.; Teherani, T. *J. Phys. Chem.* **1980**, *84*, 1262.
- (235) Uribe, F. A.; Sawada, T.; Bard, A. J. *Chem. Phys. Lett.* **1983**, *97*, 243.
- (236) Hasing, J. *Ann. Phys.* **1940**, *37*, 509.
- (237) Aulich, H.; Baron, B.; Delahay, P.; Lugo, R. *J. Chem. Phys.* **1973**, *58*, 4439.
- (238) Haberland, H.; Ludewigt, C.; Schindler, H.-G.; Worsnop, D. R. *Surf. Sci.* **1985**, *156*, 157.
- (239) Lee, G. H.; Arnold, S. T.; Eaton, J. G.; Sarkas, H. W.; Bowen, K. H.; Ludewigt, C.; Haberland, H. *Z. Phys. D* **1991**, *20*, 9.
- (240) Kondow, T.; Nagata, T.; Kuchitsu, K. *Z. Phys. D* **1989**, *12*, 291.

- (241) Tsukada, M.; Shima, N.; Tsuneyuki, S.; Kageshima, H.; Kondow, T. *J. Chem. Phys.* **1987**, *87*, 3927.
- (242) Lee, I. R.; Lee, W.; Zewail, A. H. *ChemPhysChem* **2008**, *9*, 83.
- (243) Takasu, R.; Hashimoto, K.; Fuke, K. *Chem. Phys. Lett.* **1996**, *258*, 94.
- (244) Takasu, R.; Misaizu, F.; Hashimoto, K.; Fuke, K. *J. Phys. Chem. A* **1997**, *101*, 3078.
- (245) Steinbach, C.; Buck, U. *J. Chem. Phys.* **2005**, *122*, 134301.
- (246) Barnett, R. N.; Landman, U.; Cleveland, C. L.; Kestner, N. R.; Jortner, J. *Chem. Phys. Lett.* **1988**, *148*, 249.
- (247) Balabaev, N. K.; Lakhno, V. D. *Chem. Phys. Lett.* **1995**, *240*, 585.
- (248) Lee, G. H.; Arnold, S. T.; Eaton, J. G.; Sarkas, H. W.; Bowen, K. H.; Ludewigt, C.; Haberland, H. Z. *Phys. D* **1991**, *20*, 9.
- (249) Smyth, C. P.; Hitchcock, C. S. *J. Am. Chem. Soc.* **1934**, *56*, 1084.
- (250) Liu, Q. L.; Wang, J. K.; Zewail, A. H. *Nature* **1993**, *364*, 427.
- (251) Bell, I. P.; Rodgers, M. A. J.; Burrows, H. D. *J. Chem. Soc., Faraday Trans. 1* **1977**, 315.
- (252) Xia, C.; Peon, J.; Kohler, B. *J. Chem. Phys.* **2002**, *117*, 8855.
- (253) Shkrob, I. A.; M. C. Sauer, J. *J. Phys. Chem. A* **2002**, *106*, 9120.
- (254) Takayanagi, T. *J. Chem. Phys.* **2005**, *122*, 244307.
- (255) Timerghazin, Q. K.; Peslherbe, G. H. *J. Phys. Chem.* **2008**, *112*, 520.
- (256) Azar, J.; Kurlancheek, W.; Head-Gordon, M. *Phys. Chem. Chem. Phys.* **2011**, *13*, 9147.
- (257) Gutowski, M.; Skurski, P.; Jordan, K. D.; Simons, J. *Int. J. Quantum Chem.* **1997**, *64*, 183.
- (258) Gutowski, M.; Jordan, K. D.; Skurski, P. *J. Phys. Chem. A* **1998**, *102*, 2624.
- (259) Lide, D. R. In *CRC Handbook of Chemistry and Physics*; 90th ed.; Lide, D. R., Ed.; CRC Press/Taylor and Francis: Boca Raton, FL, 2010.
- (260) Takayanagi, T.; Hoshino, T.; Takahashi, K. *Chem. Phys.* **2006**, *324*, 679.
- (261) Ehrler, O. T.; Griffin, G. B.; Young, R. M.; Neumark, D. M. *J. Phys. Chem. B* **2009**, *113*, 4031.
- (262) Koch, D. M.; Peslherbe, G. H. *Chem. Phys. Lett.* **2002**, *359*, 381.
- (263) Markovich, G.; Pollack, S.; Giniger, R.; Cheshnovsky, O. *J. Chem. Phys.* **1994**, *101*, 9344.
- (264) Takayanagi, T. *J. Phys. Chem. A* **2006**, *110*, 7011.
- (265) Takayanagi, T. *Chem. Phys.* **2004**, *302*, 85.
- (266) Burrow, P. D.; Michejda, J. A.; Jordan, K. D. *J. Chem. Phys.* **1987**, *86*, 9.
- (267) Jordan, K. D.; Burrow, P. D. *Acc. Chem. Res.* **1978**, *11*, 341.
- (268) Christophorou, L. G.; Goans, R. E. *J. Chem. Phys.* **1974**, *60*, 4244.
- (269) Han, S. Y.; Song, J. K.; Kim, J. H.; Oh, H. B.; Kim, S. K. *J. Chem. Phys.* **1999**, *111*, 4041.
- (270) Ando, N.; Mitsui, M.; Nakajima, A. *J. Chem. Phys.* **2008**, *128*, 154318.
- (271) Song, J. K.; Lee, N. K.; Kim, S. K. *J. Chem. Phys.* **2002**, *117*, 1589.
- (272) Song, J. K.; Lee, N. K.; Kim, J. H.; Han, S. Y.; Kim, S. K. *J. Chem. Phys.* **2003**, *119*, 3071.
- (273) Klug, D. D.; Whalle, E. *Can. J. Chem.* **1973**, *51*, 4062.
- (274) Bedard-Hearn, M. J.; Larsen, R. E.; Schwartz, B. J. *J. Chem. Phys.* **2005**, *122*, 134506.
- (275) Bowron, D. T.; Finney, J. L.; Soper, A. K. *J. Am. Chem. Soc.* **2006**, *128*, 5119.
- (276) Shoshana, O.; Lustres, J. L. P.; Ernsting, N. P.; Ruhman, S. *Phys. Chem. Chem. Phys.* **2006**, *8*, 2599.
- (277) Cavanagh, M. C.; Young, R. M.; Schwartz, B. J. *J. Chem. Phys.* **2008**, *129*, 134503.
- (278) Bragg, A. E.; Schwartz, B. J. *J. Phys. Chem. B* **2008**, *112*, 483.
- (279) Bragg, A. E.; Schwartz, B. J. *J. Phys. Chem. A* **2008**, *112*, 3530.
- (280) Shreve, A. T.; Elkins, M. H.; Neumark, D. M. Private Communication.